Review article

Check for updates

Multifunctional high-entropy materials

Liuliu Han [1] ✉, Shuya Zhu[2], Ziyuan Rao [1], Christina Scheu[1], Dirk Ponge[1], Alfred Ludwig [3] ✉, Hongbin Zhang[4], Oliver Gutfleisch[1,4], Horst Hahn [5,6], Zhiming Li [2] & Dierk Raabe [1] ✉

Abstract

Entropy-related phase stabilization can allow compositionally complex solid solutions of multiple principal elements. The massive mixing approach was originally introduced for metals and has recently been extended to ionic, semiconductor, polymer and low-dimensional materials. Multielement mixing can leverage new types of random, weakly ordered clustering and precipitation states in bulk materials as well as at interfaces and dislocations. The many possible atomic configurations offer opportunities to discover and exploit new functionalities, as well as to create new local symmetry features, ordering phenomena and interstitial configurations. This opens up a huge chemical and structural space in which uncharted phase states, defect chemistries, mechanisms and properties, some previously thought to be mutually exclusive, can be reconciled in one material. Earlier research concentrated on mechanical properties such as strength, toughness, fatigue and ductility. This Review shifts the focus towards multifunctional property profiles, including electronic, electrochemical, mechanical, magnetic, catalytic, hydrogen-related, Invar and caloric characteristics. Disruptive design opportunities lie in combining several of these features, rendering high-entropy materials multifunctional without sacrificing their unique mechanical properties.

Sections

[1]Max Planck Institute for Sustainable Materials, Düsseldorf, Germany. [2]School of Materials Science and Engineering, Central South University, Changsha, China. [3]Institute for Materials, Ruhr-Universität Bochum, Bochum, Germany. [4]Institute of Materials Science, Technical University of Darmstadt, Darmstadt, Germany. [5]Institute of Nanotechnology, Karlsruhe Institute of Technology, Karlsruhe, Germany. [6]School of Sustainable Chemical, Biological and Materials Engineering, The University of Oklahoma, Norman, OK, USA. ✉e-mail: l.han@mpie.de; alfred.ludwig@rub.de; d.raabe@mpie.de

Review article

Introduction

Materials have always played a pivotal role in the development of human society. The range of accessible phase states, kinetics, transformation phenomena and properties, however, has been constrained by the fact that many materials used today are mostly based on one or two principal elements and typically use further elements only in low fractions.

Compositionally complex and high-entropy alloys (HEAs)[1–4], consisting of multiple principal elements, open up this rather limited chemical composition space. The original idea consists of stabilizing equimolar solid solutions of five or more chemical elements through enhanced configurational entropy. Today, this approach is embraced more broadly and also encompasses materials that are not (only) entropy-stabilized, targeting compositionally complex materials that have large solid solution ranges in the centre regions of multicomponent phase diagrams[5–8]. This is because, first, only a few fully random and thermodynamically stable solid solution HEAs have been identified so far, and second, some compositionally complex materials are enthalpy-stabilized rather than entropy-stabilized, for example some ionic materials. Furthermore, most of these materials are metastable and are prone to decompose into several stable phases. Beneficial properties have, in part, emerged from random solid solution states (such as high distortions and atomic-scale symmetry breaking), ordering effects and precipitation. These features allow the introduction of kinetics, microstructure and processing as additional degrees of freedom for material design. It is also understood today that HEAs do not need to be equimolar in their composition, provided that no single matrix element prevails, making the design approach much more versatile. It is further important to note that the design approach works for the bulk and for internal interfaces and surfaces. Interfaces can be as important as the bulk for certain materials, such as catalysts, hard magnets, topological materials or coatings. The two are chemically connected under near-equilibrium conditions because the partitioning and mixing states of adjacent regions depend on each other, as stated by the Gibbs adsorption isotherm.

These examples of 'relaxed-constraints' design opportunities for multicomponent materials thus give access to a wide range of continuously variable chemical compositions and properties and bring a large variety of additional microstructural phenomena into play[9]. In the latter context, kinetics, non-equilibrium phase transformations, and many chemical ordering and decoration phenomena produce a rich underlying lattice defect cosmos (point defects, dislocations, stacking faults, interfaces, surfaces and so on), providing an additional versatile material design toolbox[10–13]. The resulting microstructures can differ profoundly from those in conventional alloys because the lattice defects can be chemically highly decorated, which can be used to alter their kinetic, thermodynamic and functional features[14,15].

The latter point requires explanation: the Gibbs adsorption isotherm[16] and its kinetic analogues, such as the McLean isotherm[17], state that the driving force for solute decoration to lattice imperfections comes from the reduced self-energy of the defect affected. This seems to suggest that the total magnitude of the decoration might be similar for defects in massive and dilute solid solutions, or that the element with the highest segregation tendency (usually the element with low solubility and sufficiently high mobility) dominates the decoration. However, two theoretical considerations (and quantitative experimental findings about intense co-decoration based on atom probe tomography[15,18]) show that the magnitude of defect decoration can be higher in massive solid solutions. First, the magnitude of the chemical potential of the decorating elements, which determines the partitioning between matrix and defects, is much higher in high-entropy materials (HEMs) than in dilute solids. Second, classical adsorption isotherm formulations assume ideal solutions at the decorated defects, thus neglecting interactions among the segregating elements. However, the theories of compound isotherms and defect phase diagrams show that elemental interactions at co-decorated defects can lead to a higher total magnitude in (co-)segregation than in the dilute limit[19]. This, however, also implies that once highly co-segregated, these elements tend to form intermetallic or corresponding precursor phase states.

Each material design dimension offers multiple options for tuning. This qualifies HEMs as the largest uncharted material design territory, fuelling expectations to discover new materials and phenomena. The advantage of the compositional complexity concept over conventional material design principles is the possibility for large and compositionally smooth chemical variations within the solid solution, even with elements immiscible in conventional alloys (and adjacent kinetic decomposition) states. This allows the shift of alloy compositions into ranges where promising material features can be seamlessly enhanced or damped without triggering (undesired) phase transformations, a typical feature of conventional materials. The wide and continuous compositional adjustment realm offered by HEMs allows the design of the magnitude and range of a wide spectrum of physical and chemical properties within defined phase spaces, and the exploitation of the associated kinetic effects. Examples of the latter are high solute drag forces on interfaces (pinning, grain size stabilization) or pre-decoration and functionalization of grain boundaries by solutes (passivation and grain boundary protection)[20,21]. Another reason for studying compositional mixtures in materials for multifunctionality is that elements with high mutual solubility (such as Fe, Mn, Co, Ni and Cr) have a strong influence on the Fermi surface and magnetic coupling so that interesting electronic, magnetic and caloric properties are likely to be triggered[6,22–25].

This Review examines how these design options and their practically unbounded chemical adjustment opportunities can be used to create HEMs that exhibit new property spectra and reconcile multiple functionalities, including feature combinations previously thought to be mutually exclusive in conventional alloys, while retaining their often excellent mechanical properties.

Reconciling conflicting properties is a general and longstanding challenge in material design. Examples can be found in magnetic and electrically conductive materials, where functional features are often in fundamental conflict with high mechanical strength and good ductility. In metals, high flow strength and strain hardening require multiple lattice defects such as dislocations and interfaces, whereas small hysteresis, soft magnetic response and low electrical resistance require the opposite, namely, mobile magnetic domain walls and low inelastic electron scattering, respectively, both features that are adversely affected by lattice defects. This example indicates that the main reason for the conflict in realizing multifunctionality lies in the interplay among the electron, spin and lattice degrees of freedom that enable functional properties and the lattice defects required for most mechanical properties, which lead to scattering and pinning effects.

Several multifunctional compositionally complex materials have been developed so far[26,27]. Specific examples are materials combining high strength, ductility, soft magnetism and resistance to corrosion[28–31] at ambient[32–38] and high temperatures[39]; or high selectivity, activity and stability of electrocatalysts with high abundance of active sites[40–43]; or high cryogenic strength, toughness and resistance to corrosion

Review article
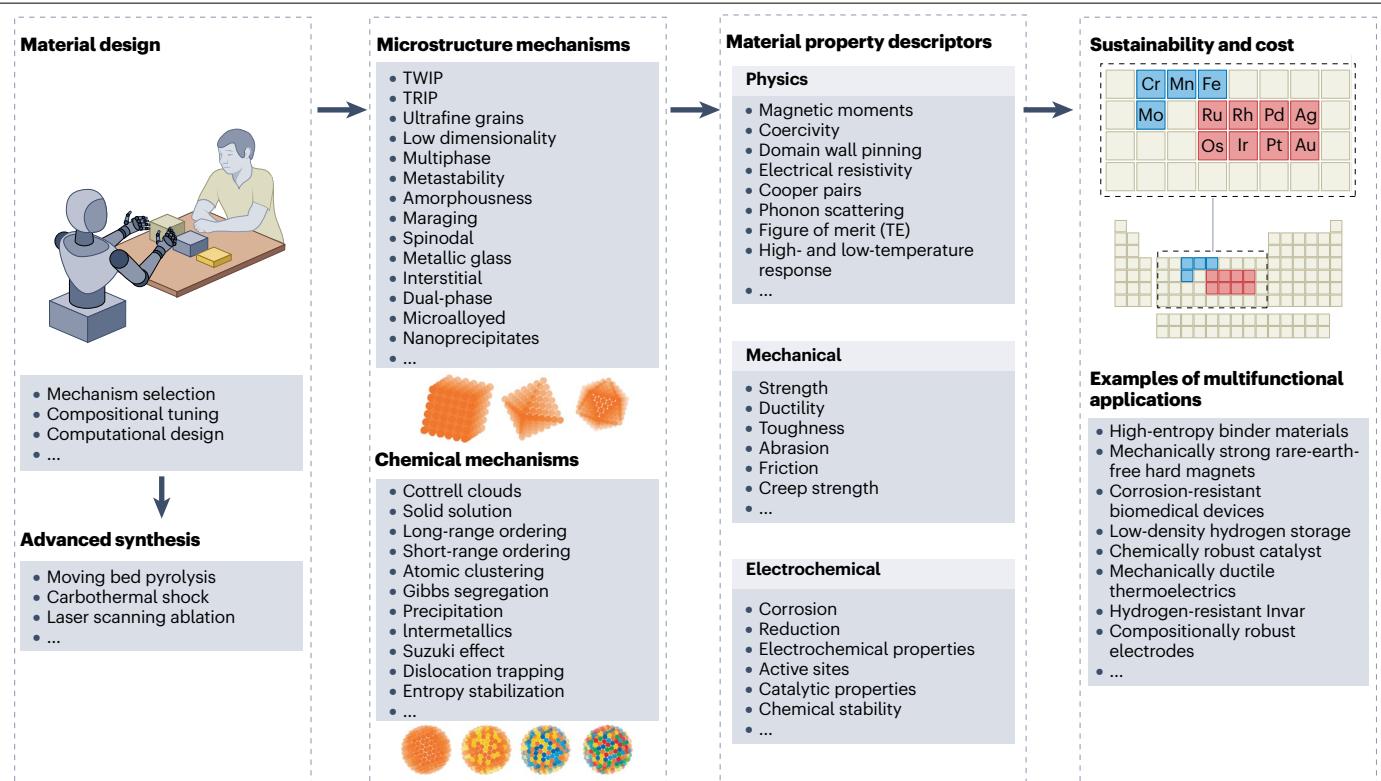
Fig. 1 | Principles, property targets, constraints and opportunities for the design of multifunctional high-entropy materials. The figure sketches some of the main aspects of the compositional and microstructural design, governing principles and synthesis methods that need to be considered for balancing multifunctionality and sustainability of high-entropy-related mechanisms with respect to realizing materials with new multifunctional property profiles, at reasonable costs and responsible use of resources. TE, thermoelectric; TRIP, transformation-induced plasticity; TWIP, twinning-induced plasticity.

and hydrogen embrittlement[44–46]. Such synergies are rarely found in low-component materials (Fig. 1).

Some of these multifunctional structure–property relations depend directly on the underlying solid solution states, such as the concentration dependence of the yield strength, the maximum magnetic moment and the electrical conductivity, whereas others, such as coercivity, also depend largely on microstructure. The more solid solution elements are brought into a metal matrix, the more degrees of freedom arise for functional tuning and for stabilizing defects through chemical decoration. This means that access to new functional properties becomes easier with higher solid solution content and variability of microstructure, and the spectrum of accessible non-equilibrium states becomes richer.

In this Review, we critically analyse and group the observed phenomena in multifunctional HEMs to identify governing principles, mechanisms and correlations common to such compositionally complex solids, with a focus on identifying the underlying scientific principles and synergies of functional compositionally complex materials. We begin with materials with a lower number of functionalities to tune (such as electrical resistivity and conductivity, and thermal expansion) and then proceed to more complex multifunctional cases such as thermoelectrics, hard magnets and catalysts. A few important methodological aspects are also discussed, such as high-throughput and artificial intelligence (AI)-assisted material design, and sustainability. The former is critical for efficiently identifying new materials when exploring this high-dimensional phase space. The latter is essential because many elements used in HEMs are forbiddingly expensive and are associated with high greenhouse gas emissions.

Design challenges and strategies for multifunctional HEMs
Discovering new multifunctional HEMs by high-throughput methods and AI
The multitude of states accessible to atoms in a HEM, considering all kinematic and chemical degrees of freedom, spin orientations, electronic excitations and configurational attributes, is huge[47,48]. Adding to this the vast array of states created by the microstructural and processing cosmos with all its defect types, it culminates in a virtually boundless set of variants, as can be formally shown in terms of the corresponding partition functions for such materials.

Consequently, screening this vast space for new multifunctional materials, microstructures and processing pathways requires disruptive support by AI, data-driven methods and high-throughput screening[49–53]. Chemical composition, microstructure and processing can all have essential roles in the design of HEMs[5]. Therefore, classical computational high-throughput approaches based on thermodynamics or quantum mechanics alone are insufficient to search for new HEMs[54,55], and phenomenological and empirical knowledge must also be considered. The identification of new equilibrium material crystal structures with complex chemical compositions is increasingly being addressed

Review article

by machine learning (ML) methods that use high-throughput electronic calculations and experimental structure data[56]. By contrast, the wide realm of non-equilibrium phenomena, such as those prevalent in microstructure and process design, is more challenging to consider in such a systematic ML-enhanced search[51,57–61]. Combinations of text mining via large language models in conjunction with agent methods, retrieval-augmented generation and graph theory might offer promising avenues for analysing cumulative knowledge from the literature and generating pathways towards active-learning-based (autonomous) material discovery[51,62]. This means that large language models will in future probably be used not as autonomous problem solvers in this field but rather to set up automated workflows that combine different ML techniques with established databases and classic simulation methods and operate them as autonomously as possible. This enhances them from stand-alone solvers into workflow automation techniques. Active learning is likely to remain a necessary approach for HEM research in the near future, because for complex scientific questions, most of the ground-truth content must still be labelled by a scientist.

As an example, a large language model approach was used for designing HEMs with up to eight principal elements[63]. The abstracts of 6.4 million papers were analysed, introducing a 'context similarity' method by leveraging text mining to identify suitable chemical elements for HEM design[64]. This technique addresses the limitations of conventional data mining methods by focusing on the mutual solubility of elements, a key factor in the design of HEMs. The work demonstrated the effectiveness of the approach by identifying several known HEMs and suggesting nearly 500 promising lightweight HEMs out

of 2.6 million possible candidate compositions, some of which were picked up in further works[65]. Another study used an active-learning strategy to accelerate the design of Invar HEMs[66]. This closed-loop approach integrates ML with density functional theory, thermodynamic calculations and experiments. After processing and characterizing 17 new alloys from millions of compositions, a subset of Invar HEMs with extremely low thermal expansion coefficients was identified.

Overviews of the use of AI methods to identify new HEMs can be found in refs. 50,51,67,68. Yet, beyond the promising opportunities sketched in these papers, there are critical aspects to consider: current multipurpose large language models have been primarily trained on 'medium-quality' corpora for alloy compositions and properties, using scientific abstracts, public webpages and open-access databases. Thus, they sometimes fail to deliver information of deeper scientific context, causality and comprehensive insight, which requires accessing the full content of quality-controlled publications, technical reports, digitized laboratory notebooks and commercial databases. Further progress in this field will rely on full publication and data content (for example, from self-archiving preprint servers and open-access publications) available to large language models combined with graph models, retrieval-augmentation and agents. Such combined approaches would equip models with higher-quality information and would be likely to enable better domain-grounded discovery of promising connections among chemical elements, materials, mechanisms, microstructures, properties and processing, which might otherwise be hard to extract. In addition, negative and outlier data need to be considered; otherwise, the AI training will be biased. In Fig. 2, we present the functional features
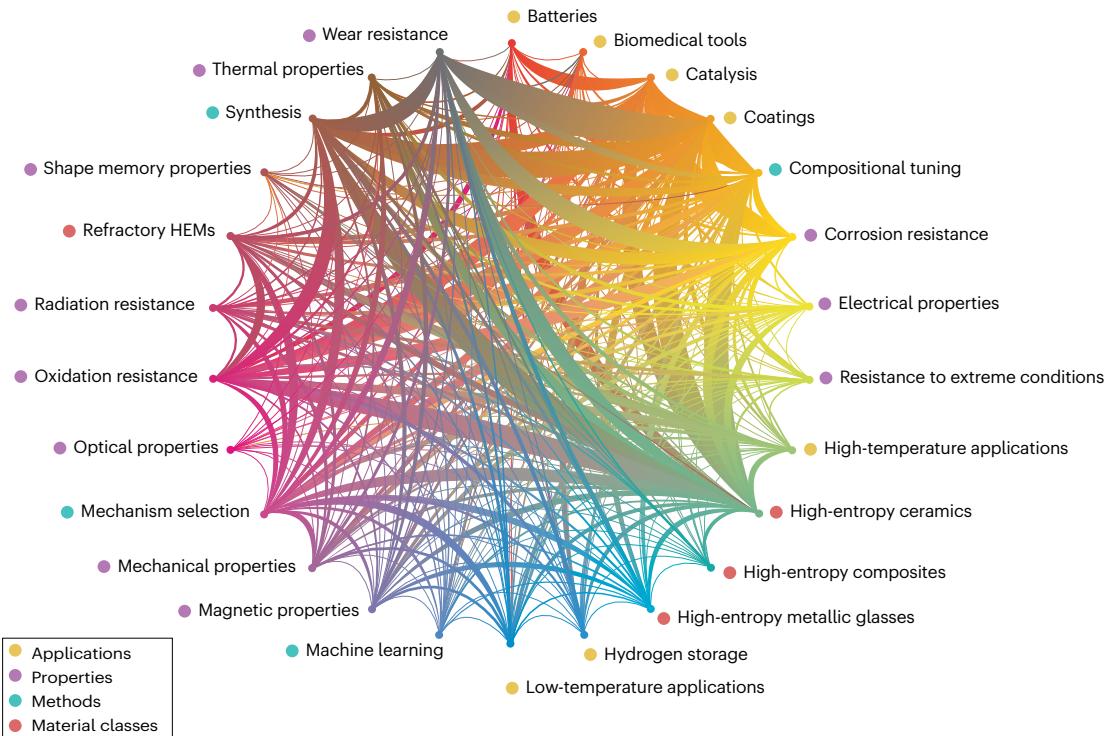

Fig. 2 | Functional features of high-entropy materials and connections between them as identified by a natural language analysis. Overview of properties explored of functional high-entropy materials (HEMs), showing promising connections among different functional characteristics of HEMs, which reveal avenues for multifunctional material design. The width of the lines indicates stronger (coarser) and weaker (finer) connections among different characteristics.

Review article

of HEMs (apart from their widely studied mechanical properties) and the connections between them, as identified by a natural language analysis (Supplementary section 1 and Supplementary Fig. 1). The analysis used more than three million texts from the HEM literature, revealing interesting feature links, which might help to catalyse further discovery of multifunctional HEMs.

Achieving and optimizing a multifunctional property spectrum

The fundamental design challenge of HEMs lies in reconciling multifunctional properties in one material while avoiding property conflicts. Therefore, understanding the mechanisms underlying the conflicting properties is key. Here, we consider the electronic, magnetic and electrochemical features of the materials as well as additional microstructure-based effects in the design strategies to exploit their respective degrees of freedom without counteracting multifunctionality.

Important structure-dependent and composition-dependent material properties are thermodynamic stability, kinetics and transport, spontaneous magnetization, Curie temperature, electrical and thermal conductivity, free energy landscapes of the phases, and the features of catalytic surfaces. These are mainly determined by the chemical compositions and the phase components as a function of temperature and pressure. Thermodynamic modelling and density functional theory, in conjunction with ML-based methods, can calculate these features, as predictors for pre-screening the large composition space before doing experiments. Examples are the accelerated design of high-entropy Invar alloys, high-entropy metallic glasses[69] and HEMs for enhanced electrocatalytic oxygen reduction[70]. In addition, multifunctional properties[71] can be optimized simultaneously by evaluating the Pareto front through a multiobjective optimization strategy[72].

The microstructure of a material provides additional entry points for property shaping, for example by introducing microstructural features across different length scales. As an example, introducing well-tuned and controlled precipitates larger or smaller than the magnetic domain wall width in soft magnetic HEMs can improve mechanical strength without increasing coercivity. Non-homogeneous, structurally and chemically graded HEMs consisting of regions with varying mechanical or physical properties could also provide property synergies beyond the rule-of-mixtures[35,73,74]. In addition, multiple-length-scale microstructure design can be supported by scale-bridging simulations. For instance, ML-enhanced interatomic potentials can bridge density functional theory calculations and mesoscale modelling[75], thus providing a framework to simulate the interplay between all degrees of freedom.

Magnetic HEMs
Boundary conditions for HEMs with improved magnetic properties

Materials with spontaneous ordering of their magnetic moments along the same direction below the Curie temperature (T_c) are referred to as ferromagnetic. The physical origin of ferromagnetism is the quantum-mechanical exchange interaction. The magnetic moments of transition metals are mainly governed by the spin and orbital motion of unshielded electrons in the outermost subshell, particularly near the Fermi level. The maximum magnetic moment per unit volume when all magnetic moments are aligned along the direction of the external magnetic field is the saturation magnetization (M_s) or polarization (J_s).

The degree to which the material can withstand an opposing external magnetic field without being demagnetized is quantified by the coercivity (H_c). The upper limit of this property is the anisotropy field. The connection between the saturation magnetization and coercivity is the microstructure. The shape of the hysteresis loop and the value of coercivity are used to categorize soft ($H_c < 1$ kA m^{-1}), semihard (1 kA m$^{-1} < H_c < 10$ kA m^{-1}) and hard ($H_c > 10$ kA m^{-1}) magnetic materials, although these are only rough material classes, and market demand exists today for materials with practically any type and shape of hysteresis. Soft and hard magnets are key components in advanced energy conversion, electromobility, smart grids, electrification of transport and industry, data storage and more. Multifunctional magnets with high longevity are increasingly required to operate safely and efficiently even when parts are exposed to harsh mechanical and corrosive conditions. HEMs can play a pivotal role in that respect, owing to the vast material space that can be explored in chemical composition, continuous mixing of magnetically coupling elements and microstructure design to obtain a wide variety of properties[22,47,48,76] (Fig. 3a). Moreover, the lattice defects that make up the microstructure and extend over several length scales (Fig. 3b) can interact efficiently with the characteristic micromagnetic length scales.

Soft magnetic properties based on the HEM concept

Interesting design opportunities for magnetic HEMs come from the large (and hence tunable) solid solution ranges of transition metal mixtures with strong magnetic moments such as Fe, Co, Ni, Mn and Cr, with the former three being ferromagnetic and the latter two being paramagnetic and antiferromagnetic at room temperature, respectively. The advantage of such solutes, particularly with respect to soft magnetic features, is the moderate interaction between solutes and domain wall motion, which results in low coercivity and low hysteresis losses under alternating magnetic fields and enables tuning of the material's electrical resistivity, an important feature for transformers and motors, where eddy current losses should be minimized. The attractiveness of this alloy system lies in its good mechanical and corrosion properties, showing that multifunctional magnetic HEMs are possible.

Some studies[77,78] have summarized the key magnetic properties of HEMs in terms of M_s and H_c covering a wide composition space. Most of these magnetic HEMs contain a major fraction of ferromagnetic elements to provide ferromagnetism based on the ternary system Fe–Co–Ni. We compare the M_s against H_c of HEMs and of commercial magnetic materials in Fig. 4. The M_s values of HEMs with face-centred cubic (fcc) crystal structures are comparable to those of conventional Fe–Ni alloys (~100–150 A m^2 kg^{-1}). The addition of auxiliary elements for achieving multiproperty requirements usually leads to a decrease in the density of the magnetic moments and hence in M_s. The effect of different alloying elements on the magnetic properties has been screened, including for C (ref. 79), Al (refs. 80,81), Si (refs. 82,83), Mg (ref. 83), Cr (ref. 84), Cu (ref. 85), Mn (ref. 86), Co (ref. 86), V (ref. 87), Ti (ref. 88), Ag (ref. 89), Pt (ref. 89), Mo (ref. 89), Sn (refs. 90,91), Ge (refs. 88,90), Ga (ref. 91) and Ce (ref. 79).

As M_s depends on the chemical composition, crystal structure and electronic properties, enhancing M_s while using a less complex and expensive chemical composition is an essential yet challenging design task. A further promising aspect of exploiting compositional complexity lies in stabilizing ferromagnetic ordering and electron-spin coupling at the Fermi level through alloying. As an example, the room-temperature M_s of equiatomic FeNiCoMn increased by 77% and 177% on adding 10 at% and 20 at% of non-magnetic Cu, respectively[25].

The increase in M_s is associated with forming a ferromagnetic Fe–Co rich phase stabilized by Cu. In addition, alloying enables phase engineering by forming stronger ferromagnetic components in higher-volume fractions. Introducing a strong ferromagnetic body-centred cubic (bcc) phase by adding Al into fcc CoFeMnNi enhanced the M_s from 18 A m² kg⁻¹ to 148 A m² kg⁻¹ (ref. 91). The mechanisms behind these counterintuitive strategies lie in the change in chemical composition, electronic structure at the Fermi level, unit-cell volume paired with elastic stresses, and the related magnetic ordering, suggesting that non-ferromagnetic elements can also contribute to tuning the magnetic properties of HEMs.

Most reported HEMs show relatively high H_c (~0.1–10 kA m⁻¹, Fig. 4). Based on the grain-size dependence of the coercivity (which is proportional to the sixth power of the grain size)⁹², low H_c values can be obtained by realizing a nanocrystalline structure (<50 nm). By contrast, larger grain sizes have the advantage of allowing domain wall motion with lower energy losses and having higher permeability and better thermal stability than small grains.
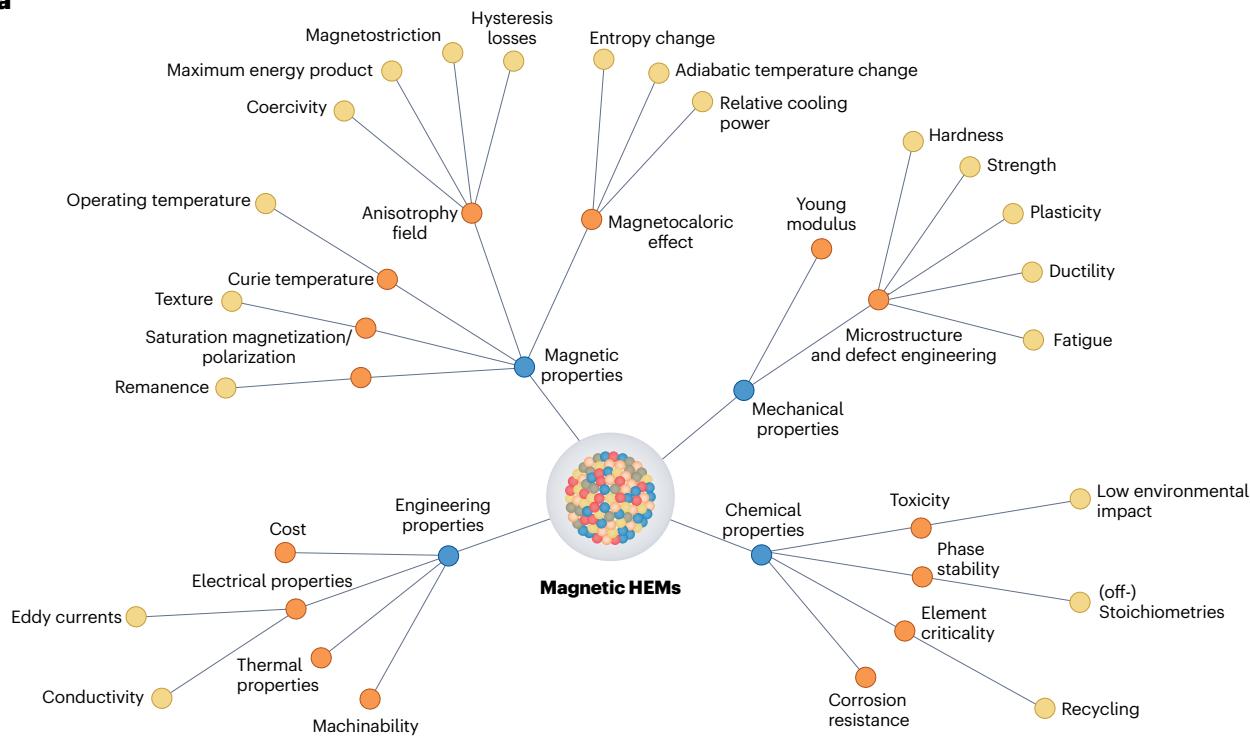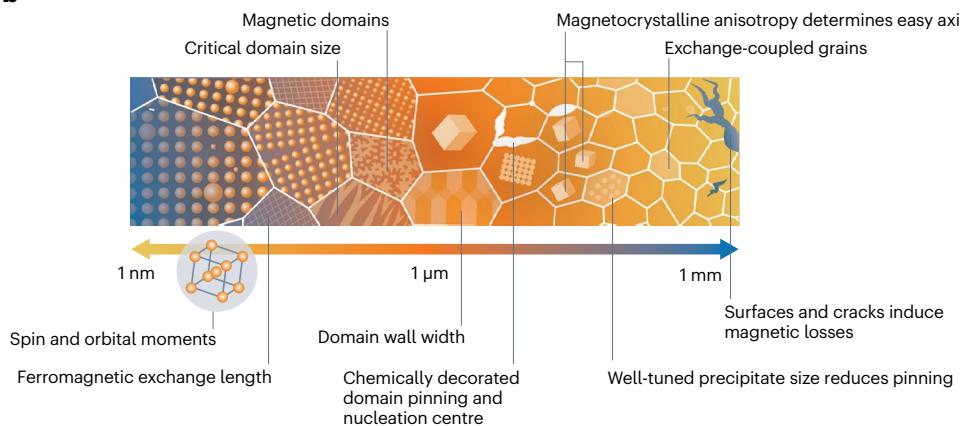

Fig. 3 | Magnetic high-entropy materials. a, Sketch of the primary functional (orange) magnetic and important secondary (yellow) properties for soft and hard magnets and magnetocaloric materials. **b**, Length scales of different defects responsible for magnetic and mechanical properties exploited in the high-entropy material (HEM) concept.
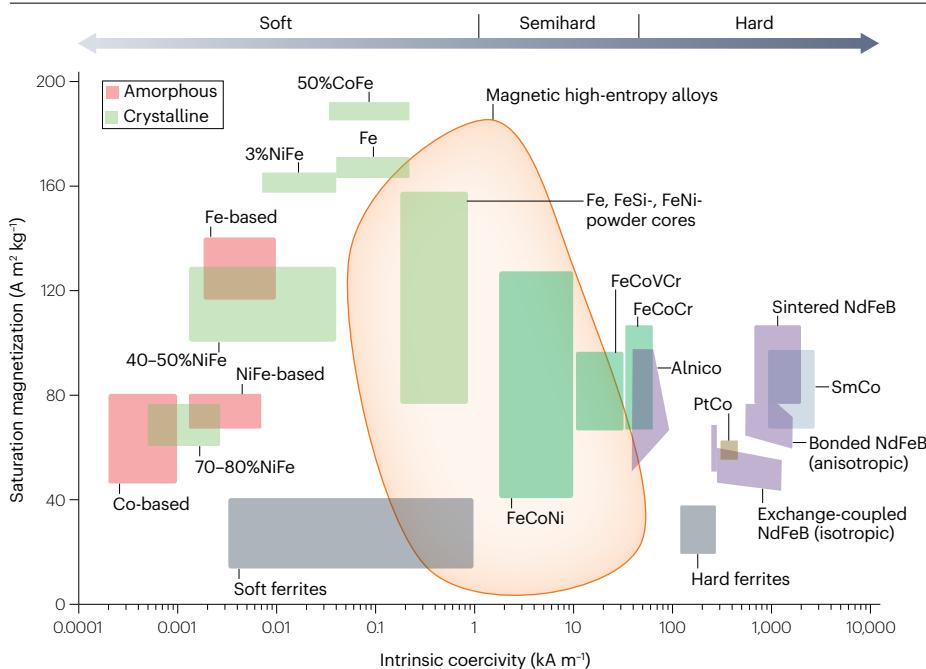
Fig. 4 | Magnetic properties of high-entropy materials. Saturation magnetization versus coercivity for several magnetic high-entropy materials (HEMs) compared with values for various soft and hard magnetic materials. Adapted with permission from ref. 260, Wiley.

A caveat to realizing these features in HEMs lies in the relatively high internal stress levels of such alloys, arising for example through a low stacking-fault energy and the resulting complex microstructures, which can increase coercivity. Nanocrystalline Co–Cu–Fe–Ni–Zn with grain sizes of ~5–20 nm was shown to have a high H_c of 1.6 kA m^{-1} (ref. 93). The formation of an additional incoherent microscale phase through co-alloying of Al and Si in Fe–Co–Ni–(Al–Si)$_x$ (grain size ~200 μm) from $x = 0$ (fcc) to $x = 0.3$ (fcc + bcc) led to a significant increase in H_c from 1.0 kA m^{-1} to 19.3 kA m^{-1} (ref. 94).

So far, few soft magnetic HEMs have surpassed the properties of commercial materials in terms of magnetic performance and cost[37,39]. However, the limitation of conventional soft magnetic materials is that they cover a relatively narrow feature portfolio. New alloy variants must be tuned for multifunctional property profiles to meet demanding engineering needs arising from harsh service conditions, such as mechanical loads and corrosion. These include high and dynamic mechanical stresses, high or cryogenic temperatures, wear, corrosion and hydrogen exposure. This poses new fundamental design challenges because most mechanical strengthening and corrosion protection methods introduce lattice defects, phases and internal stress fields that can pin the motion of magnetic domain walls, thus increasing coercivity and the associated hysteresis losses.

A few attempts have been made to address such challenges and to develop HEM-based soft magnetic materials that reconcile multiple properties[31,33,36,95]. Certain types of second-phase precipitates can enhance mechanical strength without sacrificing coercivity. For example, introducing coherent nanoprecipitates into fcc Fe–Co–Ni–Ta–Al increased the yield strength from ~500 MPa (no precipitates) to ~1,200 MPa (average nanoparticle size ~5–13 nm) while maintaining ductility (tensile elongation >15%)[38]. The pinning of the domain wall motion by nanoprecipitates (size below Bloch wall thickness) was found to be much smaller than that resulting from high-angle and twin boundaries, yet the coercivity slightly increased from 0.6 kA m^{-1}

to 0.8 kA m^{-1}. This is because the type, composition, volume fraction and shape of the precipitate leave room for optimization.

Further investigations addressed the compositional and microstructural evolution of nanoprecipitates in Fe$_{32}$Ni$_{28}$Co$_{28}$Ta$_5$Al$_7$ (ref. 37) to understand their effect on mechanical and magnetic properties (Fig. 5a). Two effects were observed. First, the internal stress level gradually decreases through the coarsening of the nanoprecipitates during isothermal heat treatment. This is driven by the reduction in the specific surface area, elastic lattice misfit and associated coherency stresses. While the coherency misfit between matrix and nanoprecipitates slightly increases for each particle, the total elastic distortion and interface area become smaller because of competitive coarsening. Second, further coarsening of the nanoprecipitates increases the magnetostatic energy, and strong pinning arises when the nanoprecipitate size approaches the domain wall width. These features were balanced by a well-tuned nanoprecipitate size of ~90–100 nm, enabling an extremely low coercivity of 78 A m^{-1} and a high tensile strength of 1,336 MPa at 54% tensile elongation with good saturation magnetization of 100 A m^2 kg^{-1} and high electrical resistivity of 103 μΩ cm. These properties are compared with those of commercial soft magnets in Fig. 5b.

A similar nanoparticle approach was used in HEMs containing non-ferromagnetic TiC nanocarbides uniformly dispersed in a ferromagnetic Fe–Ni–Co matrix produced by powder metallurgy[35]. The nanocarbides suppressed the grain growth in the matrix, resulting in a fine grain size (tens of nanometres to ~300 nm). The material achieved a good combination of mechanical (yield strength ~1,125 MPa at 10% ductility) and magnetic properties ($M_s \approx 107.2$ A m^2 kg^{-1}, $H_c \approx 263.1$ A m^{-1}).

These examples show that structural defects with optimal size, dispersion, morphology and composition can maximize the interaction strength with dislocations (providing strength and ductility) and minimize magnetic pinning of domain walls (thus maintaining soft magnetism). These considerations translate into two general design
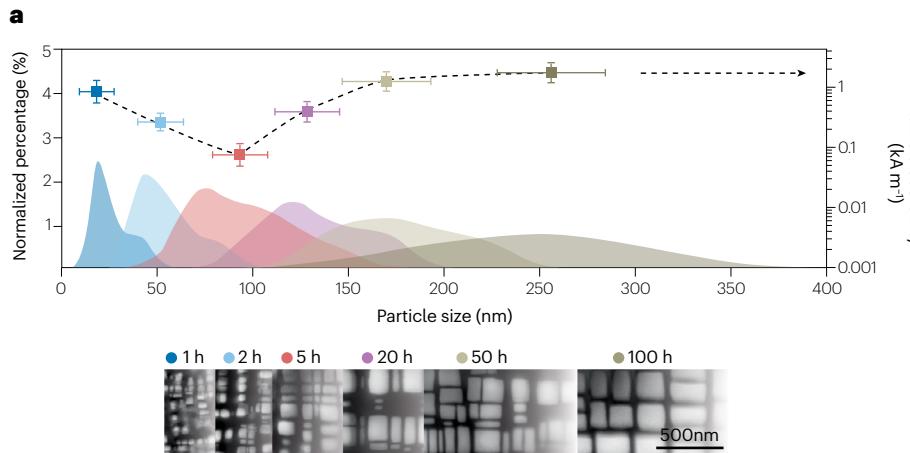
Fig. 5 | Effect of nanoprecipitates on the mechanical and magnetic properties of high-entropy materials. a, Nanoprecipitate size distribution function for $Fe_{32}Co_{28}Ni_{28}Ta_5Al_7$ (at%) exposed to different isothermal heat treatment conditions (1–100 h at 1,173 K) that result in different particle sizes. The backscattered electron micrographs show the evolution of the nanoprecipitate size with time. **b**, Comparison of the electronic, magnetic and load-bearing properties of $Fe_{32}Co_{28}Ni_{28}Ta_5Al_7$ with a nanoprecipitate size range of ~90–100 nm (5 h at 1,173 K), of a related $Fe_{28.6}Co_{28.6}Ni_{28.6}Mn_{7.1}Al_{7.1}$ compound, and of several commercial soft magnets: $Fe_{92.3}Si_{7.7}$ (converted from Fe–4Si in wt%), $Fe_{22.4}Ni_{77.6}$ (converted from Fe–78.5Ni in wt%); and $Fe_{50.2}Co_{47.6}V_{2.2}$ (converted from Fe–49Co–2V in wt%). For coercivity, the outermost boundary value is the minimum coercivity of 1 A m^{-1}. Adapted from ref. 37, CC BY 4.0.
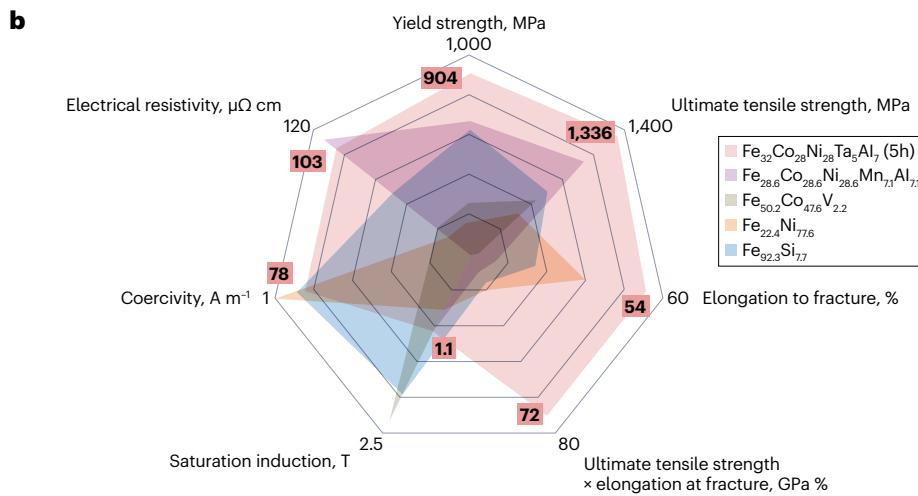
criteria. First, the chemical composition and crystal structure determine the maximum magnetization and, to some extent, the minimum coercivity that shapes the envelope of the hysteresis curve of soft magnetic HEMs. Second, microstructural features needed to improve mechanical properties should avoid strong interactions with magnetic domain walls to keep coercivity low yet allow tuning of additional properties. HEM-based nanostructuring is thus an approach that is well suited to decoupling mechanical and magnetic length scales and mechanisms (Fig. 3b) for realizing mechanically strong multifunctional soft magnets.

Hard magnetic properties based on the HEM concept

The increasing supply risks for rare-earth (RE) elements require designing high-performance RE-free hard magnets or applying HEM design principles to RE-based hard magnets.

Compared with the extensive work conducted on soft magnetic HEMs, only a few studies were dedicated to compositionally complex and multifunctional hard magnets. This is due to a fundamental design challenge: most widely studied HEMs have high crystal symmetry, a feature well suited to soft magnets but not to hard magnets, as a strong magnetocrystalline anisotropy (H_a) requires non-cubic structure

elements to obtain a high coercive force H_c. The strongest hard magnets are based on RE–transition metal intermetallics, using RE elements such as Nd, Sm, Dy and Tb, and 3d transition metals such as Fe and Co. The single-electron spin–orbit coupling constant ζ is proportional to Z^4, where Z is the atomic number. The RE elements provide strong spin–orbit coupling to achieve a high H_a and hence a large magnetic hysteresis. The 3d metals provide high spontaneous magnetization and a high Curie temperature. Cobalt and the RE metals are classified as resource-critical. RE-based hard magnets such as Nd–Fe–B (with a high magnetocrystalline anisotropy energy (MAE) of 5.0 MJ m^{-3} and M_s = 720 kA m^{-1}) and Sm–Co (MAE = 17.0 MJ m^{-3}, M_s = 910 kA m^{-1}) are the benchmark systems, opening up a sizable cost and performance disparity to other classes of commercial hard magnets such as Al–Ni–Co (MAE = 0.04 MJ m^{-3}, M_s = 50 kA m^{-1}) and ferrites (MAE = 0.03 MJ m^{-3}, M_s = 125 kA m^{-1})[96]. The MAE originates from the spin–orbit coupling and sets an upper limit for the microstructure-dependent coercivity of hard magnets. A HEM-based hard magnet filling this gap, ideally paired with other multifunctional material prerequisites, in particular resistance to harsh operating conditions, would be a challenging but truly disruptive invention. For instance, hard magnetic HEMs with good mechanical performance (particularly improved fracture toughness)

Review article

would be compatible with manufacturing methods that cannot be used for conventional RE hard magnets because of their brittleness.

Rare-earth-free hard magnetic HEMs. When moving towards RE-free magnets, that is, truly novel substitutional (or gap) magnet types, we face the fundamental challenge of inducing a sufficiently high magnetic anisotropy. In a recent review[97], four ways of enhancing the magnetocrystalline anisotropy in $3d$ magnets were specified. First, fine-tuning the number of electrons through alloying can enhance the MAE or strengthen the easy-axis anisotropy in Fe–Co alloys, for example by introducing tetragonal distortion. Second, a volume expansion of the unit cell increases T_c and enhances the spontaneous magnetization, increasing the orbital moment. Third, combining $3d$ elements with heavier $5d$ transition elements ($4f$ not considered here owing to the criticality from a material point of view and non-direct hybridization between RE-$4f$ and TM-$3d$ shells) can help to overcome the issue of small spin–orbit coupling and anisotropy of $3d$ compounds. However, many $5d$ elements are equally resource-critical and expensive. The fourth strategy is the exploration of the vast space of quaternary and quinary materials: possible metastable and/or even unknown phases might be found by high-throughput and ML-guided exploration methods.

Combining non-cubicity with the HEM concept, one could explore stabilizing tetragonality in Fe–Co–Ni–…–X compounds, where X could be H, C, B or N as interstitials. The effects of these interstitials on the MAE and orbital magnetization can be understood in terms of the local chemical bonding between them and the surrounding magnetic substitutional atoms. H, B, C and N interstitials can break the cubic symmetry, inducing a global tetragonal distortion, thus yielding an interstitially induced magnetic anisotropy. This was initially demonstrated for cubic full Heusler compounds based on a detailed analysis of the Bain path and on the atom-resolved MAE, which showed corresponding changes in the local crystalline environment[98]. This strategy could provide an efficient way to design hard magnets.

An advance in the development of RE-free (semi-)hard magnetic HEMs was the discovery of $Fe_2CoNiAlCu_{0.4}Ti_{0.4}$ (ref. [99]). Compared with the commercial alloy Alnico 2 under isotropic conditions ($H_c \approx 46.3$ kA m^{-1}, $(BH)_{max} \approx 1.70$ MG Oe), this HEM has a higher H_c of 86.0 kA m^{-1} and a $(BH)_{max}$ of 2.06 MG Oe. Subsequent work further improved H_c to 101.4 kA m^{-1} via altering the chemical shape anisotropy of nanoprecipitates by magnetic annealing[100].

Another avenue of research pertains to the FeCoNiAl system with tunable magnetic and mechanical properties. Half-replacing Co by Cr in $Co_xCr_{1-x}FeNiAl$ (ref. [101]) increases H_c from 1.1 kA m^{-1} to 7.6 kA m^{-1}, yet M_s decreases from 100 A m^2 kg^{-1} to 46 A m^2 kg^{-1}. Introducing eutectoid-like nanolamellar nanoprecipitates in $CoFeNiAl_{0.3}$ (ref. [102]) via isothermal heat treatment increases the H_c, M_s and Vickers hardness (H_v) simultaneously from 0.2 to 12.8 kA m^{-1}, 127 to 139 A m^2 kg^{-1} and 195 to 513H_v, respectively. In-depth characterization by electron microscopy reveals that the multilength-scale phase boundary exerts strong pinning on domain wall motion[103], which is responsible for the significant increase in coercivity.

Finally, most research on magnetic HEMs is based on tailoring composition and thermomechanical processing to achieve the best performance. The future development of multifunctional magnetic HEMs should be combined with advanced computational tools (such as ML[104,105]) and experimental tools (such as in situ observations of material response triggered by a magnetic or temperature stimulus). The former can help to improve the efficiency and speed of alloy design and maturation through data-driven correlation

studies and/or causal mechanism understanding, and the latter can help to uncover fundamental structure–property relationships down to the single-defect level. In addition, scientific questions regarding the interaction between microstructure and magnetic features need to be answered: for example, the magnetism at the ground state calculated by computational methods is limited to small system sizes and several magnetic configurations. Another challenge is characterizing the local interactions between magnetic and microstructural features, especially at the atomic scale.

Rare-earth-containing hard magnetic HEMs. A starting point for RE-containing hard magnetic HEMs is the 'RE-lean' intermetallic compounds, such as $ThMn_{12}$-type hard magnets. They are promising because of their magnetic properties, which surpass the benchmark material Nd–Fe–B, but face issues in terms of phase stabilization. $NdFe_{12}N_x$ structures can form in thin films, but their bulk counterparts remain elusive. Substituting Fe with non-magnetic elements, although it lowers their magnetic properties, helps to stabilize the $ThMn_{12}$-type phase[106]. Interstitial nitrogen is required in bulk $Nd(Fe,X)_{12}$ to induce magnetocrystalline anisotropy. However, processing techniques such as sintering or hot compaction cannot be used, as nitrides in these systems become unstable at elevated temperatures. A related system, $Sm(Fe,X)_{12}$, shows magnetocrystalline anisotropy without nitrogenation, thus probably qualifying as a more versatile processing alternative[107,108]. Multiple alloying elements can yield stable Nd-based and Sm-based 1:12-type phases with a tailored microstructure that hinders the onset of critical magnetization reversal processes[109]. Here, an opportunity arises to explore HEM design to master both the multielement and the multifunctional complexity that affect phase stability, magnetic moments and microstructure-dependent coercivity effects[110].

The benefits of applying the HEM concept on the RE site in a RE-based hard magnetic intermetallic compound remain to be explored. Using a natural RE element distribution from a monazite or bastnäzite ore, the 'RE ore basket', might be a promising approach. Similarly, the use of a RE mischmetal composition (55% Ce, 25% La, ~15–18% Nd) might offer a worthwhile avenue for the synthesis of hard magnetic HEMs.

Magnetocaloric HEMs

The magnetocaloric effect (MCE) is the reversible change in the thermodynamic variables of a material – temperature (T) and entropy (S) – as a result of the application and removal of an external magnetic field. If this magnetization or demagnetization is performed adiabatically, heating or cooling of the material can be obtained[111–113]. The total S remains constant for this step, and the MCE manifests itself in an adiabatic temperature change, ΔT_{ad}. Alternatively, by keeping T constant during magnetization or demagnetization (isothermal conditions), a transfer of thermal energy between the sample and the environment is achieved. The amount of heat transferred is $Q = T \cdot \Delta S_m$, with ΔS_m being the isothermal magnetic entropy change. The MCE is at its maximum near the phase transition temperature, where ideally the transition is sharp yet non-hysteretic, that is, it is on the verge of a first-order and second-order transition. Ideally, the magnetization is initially high and drops at the transition temperature.

The development of an energy-efficient and sustainable magnetic refrigerator is linked to the availability of a magnetocaloric material combining a large reversible MCE in a magnetic field of around 1 T, non-criticality and non-toxicity, as well as excellent secondary properties such as high corrosion resistance, mechanical stability

Review article

and machinability. About 90% of prototypical magnetic refrigerators use elemental heavy RE Gd or Gd-based compounds, which are highly critical and expensive. The MCE in Gd is based on a second-order phase transition, giving rise to small reversible isothermal entropy changes, which limit the transferable heat. La(Fe,Si)$_{13}$-based alloys are used as magnetocaloric heat exchanger materials, enhancing the transferable heat due to the underlying isostructural first-order phase transition. However, first-order materials are inherently prone to functional fatigue and often suffer from poor machinability, which is also true for the Fe$_2$P-type family of magnetocaloric materials[114,115]. Again, we encounter partially contradictory requirements that magnetocaloric HEMs could potentially help to resolve: some recent work in this context has focused on equiatomic compositions using RE elements[116–119], while other work considered mixtures of transition metal elements[120–124]. However, all the reported magnetocaloric HEMs[125] tend to show a gradual change in the magnetization as a function of temperature, that is, essentially a second-order phase transition. Tuning magnetocaloric HEMs towards a first-order phase transition is a fundamental challenge[126]. We consider it especially interesting to explore and extend the families of all-d-Heusler-type[127–129], MM′X-type[124,130,131], and Fe$_2$P-type compounds towards the HEM design concept, as these systems are in principle already multielement materials. An understanding of the physical mechanisms leading to an enhanced MCE, which includes both adiabatic temperature and entropy changes, as well as of the mechanical properties, needs to be developed from crystal, electronic structures, microstructure and configurational entropy considerations. Another attribute in this multifunctionality quest is corrosion resistance, because magnetocaloric heat exchange materials are exposed to millions of cycles over their lifetime, during which they are in constant contact with heat exchange fluid, typically water. Here, the HEM design concept could reconcile these multifaceted constraints. As the parameter space for the different synthesis routes (which include conventional melting, non-equilibrium and additive manufacturing) and deposition techniques, post-heat treatments and multielement space are hard to conceptualize, theory and ML guidance will be needed.

Thermal HEMs
Entropy engineering of thermoelectric HEMs
Thermoelectric materials convert thermal gradients (for example, from waste heat sources) into electricity through the Seebeck effect. Their conversion efficiency is determined by the figure of merit (ZT): $ZT = S^2\sigma T/\kappa$, where S is the Seebeck coefficient, σ is the electrical conductivity, T is the absolute temperature, and κ is the thermal conductivity[132]. This imposes specific design constraints on two main intrinsic material features when trying to enhance efficiency. First, strengthening of phonon scattering lowers the thermal conductivity and thus reduces heat equilibration to keep up the temperature gradient. Second, the mobility and density of the charge carriers should be high to enhance the electrical conductivity and the gain from electrical energy harvesting. Reconciling these correlated and, to some extent, mutually exclusive properties is a longstanding challenge owing to electron–phonon interactions[133]. In addition, when exposed to harsh environments, thermoelectric materials require multifunctional performance[134] such as high damage tolerance[135–137], oxidation resistance[138,139], good mechanical properties[140], low cost[141,142] and high cyclable temperature stability[143].

The HEM concept can be used to tune thermoelectric materials for higher conversion efficiency and safer operation[144–154]. This includes entropy engineering and composition modification. Supplementary Table 1 compares the maximum ZT values of thermoelectric HEMs and of conventional thermoelectrics. A few thermoelectric HEMs surpass the properties of commercial thermoelectric materials. This shows that entropy manipulation and composition design is a promising material design pathway to better thermoelectric properties, and also to additional multifunctional benefits.

For example, increasing the configurational entropy can stabilize solid solution ranges beyond the solubility limits of thermoelectric materials explored so far. This could be used to create higher lattice distortion, thus enhancing phonon scattering to lower the thermal conductivity. Alternatively, increasing the S and Te contents in a Pb–Sb–Se–Te–S thermoelectric HEM triggers a multiphase state due to enthalpy-driven phase separation. This multiphase structure transforms back to a single-phase state when another element, SN, is added, beyond the equilibrium solubility limit[155]. This effect was attributed to the faster increase in entropy over enthalpy when adding Sn, leading to entropy-driven structural phase stabilization. The severely distorted lattice in Pb$_{0.89}$Sb$_{0.012}$Sn$_{0.1}$Se$_{0.5}$Te$_{0.25}$S$_{0.25}$ (lattice strain ~0.45%) compared with that of the reference material (Pb$_{0.99}$Sb$_{0.012}$Se, lattice strain ~0.16%) strongly affects thermal transport, producing a high maximum ZT value of 1.8 at 900 K. Although the high configurational entropy and sluggish diffusion in HEMs can help to stabilize materials against property degradation at high temperatures[156], the possible influence of thermal cycling on thermal decomposition and the associated changes in thermoelectric performance of the reported Pb$_{0.89}$Sb$_{0.012}$Sn$_{0.1}$Se$_{0.5}$Te$_{0.25}$S$_{0.25}$ materials during service require further study.

The Seebeck coefficient of thermoelectric HEMs can be enhanced by exploiting compositional complexity and high configurational entropy. The former helps to tune electronic band features close to the Fermi level (such as band degeneracy or band convergence)[157] at optimal carrier concentration. The latter can help to produce higher-symmetry crystal structures with a larger electronic density of states and effective mass[158], especially for material systems with low initial crystal symmetry[159].

A downside of deploying the HEM concept for thermoelectrics is the decrease in electrical conductivity due to the Anderson localization of electrons in highly disordered systems[160]. This is considered a general trade-off between thermal and electrical conductivity, as expressed by the Wiedemann–Franz law. The reduced carrier concentration should be compensated by other means to enable high conversion efficiency. Recent work has shown the enhancement of thermal conductivity without sacrificing electrical properties by entropy engineering, achieving a maximum ZT value of 2.7 at 750 K in a GeTe-based HEM[147]. This was explained by the suppression of transverse phonons by localized phonons due to entropy-induced disorder. At the same time, the increased crystal symmetry delocalizes the distribution of electrons and enhances the electrical properties.

HEMs with low thermal expansion
Another research direction of HEMs is dedicated to low-thermal-expansion (Invar) materials. Thermal expansion is described by the volume change upon temperature change at constant pressure. The linear thermal expansion coefficient (TEC, α) is calculated by[161] $\alpha = \Delta L/L_0\Delta T$, where L_0, ΔL and ΔT are the initial length, change in length, and temperature difference, respectively. Low thermal expansion is required in precision instruments and for liquefied gas storage and transport[162]. The Invar alloy Fe$_{65}$Ni$_{35}$ (at%), which has a TEC value of -1.6 × 10^{-6} K^{-1} around room temperature, has been the reference for over 100 years.

Review article

The low TEC of Invar alloys is mainly attributed to spontaneous magnetostriction during the high-spin to low-spin transition. The positive thermal expansion of the lattice is assumed to be counterbalanced by the contraction induced by the magnetic transition, thus leading to a very low TEC in a certain temperature range.

However, conventional Invar alloys, such as $Fe_{65}Ni_{35}$ and $Fe_{63}Ni_{32}Co_5$, are not generally ideal materials when additional constraints such as strength, ductility, mass density, corrosion resistance and/or cost come into play. Accordingly, new Invar alloys are needed for emerging applications, in particular the cryogenic storage and transport of chemical energy carriers such as liquid hydrogen, ammonia or natural gas, which are often coupled with harsh corrosive and mechanical conditions.

Several approaches were proposed to design novel Invar-type HEMs. An active-learning strategy combining density functional theory, thermodynamic calculations and experiments enabled the design of two Invar-type HEMs[66], $Fe_{41.8}Ni_{9.4}Co_{40.9}Cr_8$ and $Fe_{54.1}Ni_{22.8}Co_{17.2}Cr_{5.9}$, with extremely low TEC around 2×10^{-6} K^{-1} at 300 K. In addition, the key strategies for designing conventional Invar alloys based on the empirical Masumoto rule, which considers M_s and T_c, are applicable to HEMs containing 3d elements[163–165]. This is because the elementary magnetic properties are mainly determined by the electronic structure, particularly near the Fermi level where the s and d states are hybridized[166,167]. Accordingly, Invar-type 3d transition HEMs can be designed by adjusting the valence-electron concentration[168].

Along similar lines, an equiatomic fcc CrMnFeCoNi alloy with a valence-electron concentration of eight electrons per atom, which is, in principle, equivalent to fcc Fe, was shown to have similar thermal expansion properties to the anti-Invar material fcc Fe, with the difference that the HEM is entropy-stabilized throughout its solid-state temperature range[165].

The thermal expansion response of $Fe_{30}Co_{30}Ni_{30}Cr_{10-x}Mn_x$ HEMs (x: 0, 5 and 10 at%) between 400 K and 1,200 K was found to be comparable to that of the Cantor reference alloy[169], while a decrease in Cr and Mn content significantly lowered the TEC by up to 45.2%.

A downside of some of these Invar alloys with potential multifunctional property profiles (and of some other multifunctional HEMs) is the high alloying costs (see Supplementary Table 2). For example, using Co instead of Ni in an alloy increases its costs by about 20% per mass fraction replaced and its carbon footprint by up to 60%. Such an increase in price and environmental impact can only be justified by a corresponding improvement in functionality. A more systematic discussion of this trade-off is provided in the 'Future perspectives' section.

Electrical HEMs

Resistive materials with small temperature coefficients of resistance (TCR) and, at the same time, high values of the electrical resistivity are important components in resistive heating and precision electronic applications such as resistors, strain gauges and thermocouples. Achieving high and constant resistivity in a specified temperature range is challenging due to temperature-dependent electron–phonon scattering. In addition, resistive electrical materials in mobile systems exposed to temperature and loading variations require multifunctional properties, including high mechanical strength, ductility, and good resistance to oxidation, fatigue and corrosion. Conventional low-cost Fe–Cr–Al alloys show a good combination of high resistivity and low TCR values. Yet the high Peierls barriers for dislocation motion in the bcc lattice tend to make them brittle. Most approaches to address this fundamental challenge — that is, increasing strength and ductility without changing or decreasing resistivity — use oversaturated solid solutions. However, when the oversaturation becomes too high, brittle phases can form, and these may harm ductility and abruptly change the electrical resistivity.

HEMs are promising as multifunctional resistive materials for several reasons[36,170–172]. First, the chemical and associated microstructural complexity (grain boundaries, nanoprecipitates, ordering effects and so on) induced by the multiple principal elements can induce high lattice distortion, increasing the inelastic scattering of conduction electrons. For instance, a FeCrAlTiSi HEM was developed with a high electrical resistivity of 183 μΩ cm, a high compressive yield strength of about 1 GPa, and a uniform compressive strain of 17% at room temperature[173]. This was achieved by introducing ordered coherent L2$_1$ multicomponent nanoprecipitates, which enhance flow stress and strain hardening. The coherent interfaces between the L2$_1$ nanoprecipitates and the bcc matrix were claimed to contribute to the high electrical resistivity, although incoherent interfaces usually have higher scattering cross-sections. Second, the complex electronic structure and high electronic scattering coefficients enable effective electron–phonon and inelastic electron scattering, thus leading to low TCR values[76,170,174–176]. Conduction electrons interact with phonons at higher temperatures (300–1,000 K) and undergo inelastic scattering at intermediate temperatures (100–300 K), whereas Kondo scattering can occur at low temperatures (0–50 K). For instance, an $Al_{2.08}CoCrFeNi$ HEM was designed with a near-constant resistivity of 117.24 μΩ cm at 4.2 K and 119.90 μΩ cm at 300 K in an ordered B2-bcc structure[177]. Third, the complex compositional and structural configuration of HEMs can equip materials with a range of strengthening and toughening mechanisms aside from improving their electrical properties. However, formability measures obtained from compression tests alone are insufficient to qualify such materials for mechanically demanding load scenarios, so tensile ductility also needs to be tested.

Recent attempts were also undertaken to study whether HEMs might qualify as superconductors (Supplementary Fig. 2). The classical Bardeen–Cooper–Schrieffer (BCS) theory of superconductivity for metals requires Cooper pairs[178], which carry the superconducting current as they move without electrical resistance. Cooper pairs can form in an undistorted lattice when phonon and lattice scattering are very small. Seeking superconductivity in metallic HEMs, characterized by highly disordered lattices, thus appears to be a counterintuitive approach[179–181]. Although superconductors might potentially profit from a multifunctional alloy design approach to reconcile superconductivity with good forming properties as well as fatigue and corrosion resistance, the lattice symmetry required by the BCS theory seems to be too highly disrupted by the compositional disorder of HEMs. Therefore, promising superconducting HEM candidates have not yet been identified. However, recent findings suggest that certain HEMs show unconventional superconductivity[182]. These differ from conventional BCS superconductors and seem to have pairing mechanisms that do not rely solely on phonon interactions and undistorted lattices. Unconventional superconductivity is assumed to emerge from other mechanisms, such as electronic correlations, magnetic fluctuations or exotic pairing symmetries, which can also exist in disordered or complex alloy systems. The disorder in HEMs could thus potentially even support the emergence of new superconducting states through mechanisms that do not rely on a perfectly undistorted lattice.

Radiation-resistive HEMs

Materials exposed to radiation need to have a multifunctional property profile to withstand stringent radiation conditions (up to 200

Review article

displacements per atom), temperature (up to 1,000 °C), stress and corrosion. This is because non-equilibrium point defects, mainly vacancies, self-interstitials and transmuted atoms, can form under extreme conditions and annihilate at other defects (particularly grain boundaries). The resulting radiation-enhanced diffusion and/or formation of higher-order defects, such as nanoporosity and dislocation loops, often cause material failure due to the change of mechanical, physical and chemical properties.

The irradiation performance of HEMs can be enhanced compared with their dilute radiation-resistant counterparts owing to the massive solid solution, entropy-driven phase stability and sluggish diffusion coefficients[183-187]. More specifically, different types of complex chemical decorated defects (point defects, dislocations and grain boundaries) with high number density and good structural stability can induce a complex correlation and high binding factors between vacancies and lattice atoms[184-186,188]. With this, they can serve as effective sinks that impede the formation, migration and accumulation of point defects (such as vacancies and self-interstitials) and the subsequent coalescence of these features into larger pores and dislocation loops and further into more complex radiation-induced defects, thus reducing damage accumulation and catastrophic defect formation[189,190]. Some of these effects were revealed in thin-film samples of a four-element single-phase bcc refractory HEM ($Cr_{15}Ta_{36}V_{11}W_{38}$)[183]. Radiation exposure at doses of up to eight displacements per atom produced no signs of radiation-induced dislocation loops but instead induced the formation of second-phase precipitates. This HEM showed good radiation resistance including negligible irradiation hardening, as well as good microstructural and thermal stability.

Another plausible mechanism for the good irradiation performance of HEMs is the local self-healing capability. Molecular dynamics simulations showed that in a NiCoCrFe HEM, enhanced thermal spikes and low thermal conductivity lowered the heat dissipation rates, increasing the local recombination efficiency[190].

The radiation-tolerant HEMs concept was recently also applied to radiation-resistant ceramics, specifically (CrNbTaTiW)C (ref. 191). In this study, no displacement damage or amorphization occurred in the material exposed to doses of up to 10 displacements per atom. The implantation of Xe showed the expected formation of bubbles, yet these were smaller than in conventional materials exposed to such conditions. However, the radiation was much lower than that required for realistic uses (>200 displacements per atom) so that further studies are required.

HEMs for shape memory actuation and multicaloric cooling

Compositional complexity can be used to design and optimize multifunctional properties in materials with reversible phase transformations, such as shape memory alloys (SMA) and ferromagnetic SMA. These materials are usually tuned for large switchable and reversible strain values. They can also be designed for uses in (multi)caloric solid-state cooling, such as elastocaloric and magnetocaloric cooling[192]. The multifunctionality of these materials lies in the possibility to couple thermal, mechanical, electric and magnetic properties, for example using magnetic fields to induce large strains for fast actuation, using resistivity as a transformation-sensor and mechanical stress, and/or magnetic or electric fields for solid-state cooling.

Controlling the hysteresis curves of these materials and making the irreversible transformation effects small is essential for optimizing their properties. One example is the minimization of the reversible phase transformation hysteresis and, with that, functional fatigue. For example, in the quaternary SMA system Ti–Ni–Cu–Pd, theory-guided design combined with high-throughput experimentation led to optimized compositions around $Ti_{50.2}Ni_{34.4}Cu_{12.3}Pd_{3.1}$ with close-to-zero thermal hysteresis[193]. Compositionally complex alloys were also designed to achieve extreme values of superelasticity, namely, up to 15% in single crystals of $Ni_{35}Co_{20}Fe_{18}Ga_{27}$ (ref. 194) and 13% in textured polycrystalline $Fe_{40.95}Ni_{28}Co_{17}Al_{11.5}Ta_{2.5}B_{0.05}$ (ref. 195). Furthermore, $Fe_{43.5}Mn_{34}Al_{15}Ni_{7.5}$ showed a low-temperature dependence on superelasticity[196]. It should be noted though that these optimized HEM alloys were quite far from their respective equiatomic compositions.

An extension of the classic SMA concept towards equimolar high-entropy SMAs (HESMAs) was proposed by Georgiy Firstov[197,198] for TiZrHfCoNiCu (refs. 135,136). Expected advantages of HESMAs compared with binary or ternary systems are increased phase transformation temperatures (high-temperature SMAs) and solid solution hardening, needed, for instance, to improve transformation reversibility, especially at high transformation temperatures.

Another group of SMAs are intermetallic compounds with B2 structure, such as the Ni–Ti-based alloys, or Heusler structured materials for the case of ferromagnetic SMAs (such as Ni_2MnGa). As mixing entropy in ordered intermetallics is lower than in solid solutions, their design principles are different. For Ni–Ti, compositional extensions towards HESMAs are related to substitutions on the lattice positions of Ni (such as Cu, Pd, Pt) and Ti (such as Zr, Hf). The ratio of Ni to Ti equivalents (base element plus all substituents) should, however, remain close to 1:1, to maintain the ordered intermetallic B2 phase state of the materials and avoid additional formation of other intermetallic precipitates[199], such that the compositional flexibility for the design of Ni–Ti-based HESMAs remains limited.

For alloys with reversible phase transformations, corresponding HEM design targets lie in optimizing the compositions within the limits of stabilizing the governing transformation phase while achieving the largest possible transformation strains at maintained material integrity and reduced fatigue. Pursuing these targets can be supported by ML to establish correlations between composition, transformation strain and transformation temperatures[200,201].

Catalytic HEMs

The polyelemental nature of HEMs provides a platform to design catalytically active materials or surfaces. Key reactions in electrolysers and fuel cells, such as the hydrogen evolution reaction, the oxygen evolution reaction and the oxygen reduction reaction, require multifunctional electrocatalysts, which need to be both active and stable and should (in future) preferably consist of sustainable elements and their oxides. HEM electrocatalysts could reconcile these conflicting requirements in one material, providing functionalities by their different constituents and tunability of properties by their specific composition. Furthermore, the unique chemically complex features and properties of HEM surfaces make them suitable for designing electrocatalysts for further important reactions such as the CO_2 reduction reaction and N_2 conversion, and also for more complex multistep and cascade reactions[202,203]. Although the unique and promising properties of HEM electrocatalysts were discovered only recently[204-206], many publications prove that HEMs are interesting new catalysts for many reactions[42,207]. The design of HEM surfaces is also a promising route for developing multifunctional materials for other electrochemical applications[207-212].

Surface regions of HEMs that form out of compositionally complex solid solutions offer unique access to a large and diverse

Review article

number of polyelemental surface atom arrangements (SAAs). SAAs are defined as the arrangement of surface and subsurface atoms (first four atomic layers) within a simple crystal structure (typically fcc) and the chemical identity of these atoms with regards to binding species and binding sites (on-top, bridge, hollow site). SAAs in HEMs are abundantly available across the surface, offering a large design space to create optimal multifunctionality, in principle, for all possible electrochemical reactions. This is because the surface binding energies for reaction intermediates can, in principle, be continuously tuned by adjusting the content and distribution of the different atom species in the SAA. By this continuous coverage of binding energy, the shapes of the 'volcano plot' representations can be expected to change accordingly and hence can assist in identifying suitable HEM surface compositions. Volcano plots are representations of the relationship between the activity trends for a range of catalysts and their ability to bind to reactants or intermediates. They help to identify an optimal balance in catalyst properties, highlighting catalysts with intermediate binding energy at the peak of the volcano, which yield the highest activity (Sabatier principle). These plots can therefore serve as search maps to find catalysts offering a good compromise between the binding energy needed for reactant adsorption and the ease of product desorption.

Conceptually, the main difference between conventional elemental or binary catalysts (hitherto the best electrocatalysts, most frequently made of scarce and expensive noble metals such as Ir, Pt and Rh) and a compositionally complex solid solution is the statistical abundance of different SAAs on their surface[41]. Within the large range of SAAs on a HEM surface, a sufficient number of SAAs with high electrochemical activity are likely to form. Active sites are atomic-scale arrangements of specific atoms on the surface that provide high electrochemical activity. Enabling the design of these active sites, HEM SAAs can overcome the limitations of conventional electrocatalysts, paving the way to sustainable catalyst materials with excellent multifunctionality in terms of activity, stability and selectivity. Most importantly, some electrochemical functionalities that can currently only be provided by using scarce noble metals could be achieved by compositionally complex solid solutions comprising few or even no noble elements[204]. The reduction or replacement of active noble metal atoms in SAAs enables tuning of the active site through its binding-energy distribution pattern[41]. Furthermore, using polyelemental SAAs to reconcile conflicting requirements, replacing some of the most active but unstable elements with more stable but less active elements, should lead to overall improved performance. Recently[213], a combined experimental and theoretical search from an eight-element noble metal space was used to identify an optimum system for the oxygen evolution reaction. It was shown that in AuIrOsPdRu, Pd improves the already known activity of Ir and Ru (oxides). Osmium improves the surface area through selective dissolution, and Au acts as a structural support for the catalyst. Depending on the applied potential and relative content of Ru, Pd and Ir (at fixed Au and Os contents), the extrapolated relative catalytic activity (within the same system) could vary by a factor of 2–3. Compositionally complex solid solutions might also overcome limitations of current catalysts such as scaling relations, and are promising for catalysing multistep or cascade reactions.

The abundance of SAAs means that for a reaction of choice, the chances of SAAs acting as active sites being present on the surface and remaining there during operation are high. This is because there is not only one perfect active site but many such possible sites close to the desired optimum catalytic activity. This circumstance suggests that such complex solid solutions might be robust regarding the synthesisability of surfaces with the right SAAs and long-term stability.

A challenge lies in efficiently exploring and exploiting the immense (surface) composition space of HEMs and their SAAs. This can be addressed by high-throughput calculations coupled with high-throughput experiments[43,70,214]. The electrochemical properties of compositionally complex solid solutions can be calculated by combining density functional theory and ML-enhanced computations[215]. Using the adsorption energy of a reaction intermediate (such as *H, *OH or *O) as a descriptor, the surface constitution of a catalyst and its electrochemical activity can be correlated. The Sabatier principle states that the decisive species involved in a reaction (that is, reactants or reaction intermediates) should neither bind too strongly nor too weakly on a surface: maximum activity can be expected for optimal binding energy.

An important issue in electrocatalysts made of complex solid solutions is to control the surface composition rather than only the volume composition: surface segregation effects need to be considered to achieve the desired surface composition. Stability is, in general, as essential as activity for electrocatalysts. Here, HEMs offer new possibilities: specifically, entropy stabilization in highly multinary HEMs[216,217] could help overcome the frequently observed duality of (good) activity versus (insufficient) stability. Furthermore, at HEM surfaces, material candidates with elements that are not mixable in the bulk state can be potentially synthesized, often using non-equilibrium methods[205], in a metastable state, offering rich design possibilities. However, metastable materials could eventually demix into competing phases during operation. This aspect touches on the important problem of insufficient long-term stability of many new catalysts. Issues include changes in the surface oxidation states, gradual environmental contamination, and 'poisoning' as well as abrasion and material loss during prolonged catalyst exposure to real reactants, including their respective contaminants. Further kinetic features are the gradual changes and consequences of surface faceting as well as nanoparticle defects, which can all influence the ageing of catalysts operating under realistic conditions. The prospects of HEMs providing a pathway to active and stable catalysts need to be assessed with in situ techniques wherever possible. There are only a few publications as yet addressing this challenge[218–221].

HEMs have also been studied for heterogeneous photocatalytic reactions. For this application, catalysts need to both absorb photons to generate electron–hole pairs and catalyse the targeted redox reactions. The motivation for studying HEMs for photocatalysis is the expectation that an increase in the number and diversity of (near-)surface elements can promote photocatalytic yield, target new reactions, create new catalytic sites, alter the electronic structure and modify the surface properties of the material. This can improve light absorption, promote surface reactions and increase efficiency. Possible mechanisms comprise generating new surface reconstruction features, a wider variety of active sites, a broader photon absorption spectrum, a tunable bandgap and enhanced charge separation[203].

HEMs have also been considered in low-dimensional form as electrocatalysts for barrier reduction for certain redox reactions relevant to energy conversion problems[222,223]. The rationale behind this approach is the good electrical conductivity and multiple catalytically active sites of certain low-dimensional compounds. The specific advantages expected from extending low-dimensional materials to chemically highly complex systems are based on the potential increase in the number of charge carriers, greater selection and diversification of active sites, lower self-diffusion rates, and improved chemical and

Review article

thermal stability in catalytic applications. Challenges exist – like for many other catalysts – in the robustness of these materials on cycling, exposure to real chemical environments, and applications in reactors with less pure reactant mixtures. Also, it must be noted that good electron mobility in planar materials is an important but insufficient feature for a successful electrocatalyst.

High-entropy hydrides for hydrogen storage

Metal hydrides are used for solid-state hydrogen storage and transport applications. They store hydrogen by absorbing it from metal to hydride and releasing it reversibly. This cycling profile can be tuned through the underlying pressure–composition isotherms. Metal hydrides need to be tailored for a multifunctional property profile, including high hydrogen storage capacity (which affects efficiency), thermodynamics of hydrogen absorption and desorption (which determines the minimum working temperature), fast charging and discharging kinetics, high cycling stability, low mass density and safe hydrogen handling.

HEM hydrides have been considered for hydrogen storage[224–228] because compositionally complex solid solutions offer possibilities for adjusting properties via chemical composition modification. Moreover, the complex microstructural features, incorporating various elements and constituent phases with different compositions, lattice distortions and crystal structures, offer a high variety and number density of trap sites for improved hydrogen storage capacity and tunable low-barrier release kinetics. Finally, reducing the dehydrogenation enthalpy and increasing entropy via the HEM concept can lower the minimum working temperature by well-designed destabilization.

This means that tuning the interstitial sites available to host hydrogen via the high-entropy effect might lead to higher storage capacity. In TiVZrNbHf, a phase transition from bcc to body-centred tetragonal and finally to fcc was observed during hydrogenation, suggesting that the high build-up of lattice strain due to the atomic size differences in this HEM results in a larger spectrum of interstitial sites for hydrogen uptake and in the formation of the body-centred tetragonal structure[229].

Another type of HEM for hydrogen storage with good reversibility and fast kinetics was reported in the C14 Laves phase[230–232]. As an example, TiZrCrMnFeNi, which contains 95 wt% of the C14 Laves phase, absorbs and desorbs 1.7 wt% of hydrogen at room temperature without activation[231], comparable with other room-temperature hydrogen-storage materials (Mg_4NiPd (ref. [233])).

However, the high mass density and poor room-temperature hydrogen storage capacity of many HEMs hinder their applications. Therefore, designing low-density HEMs with large room-temperature hydrogen storage capacity is an essential target. For example, lightweight TiMgLi-based HEMs (~2.83–4.47 g cm^{-3}) with good room-temperature hydrogen storage capacities were developed[234]: a TiVMgLi HEM (2.83 g cm^{-3}) absorbs 2.62 wt% hydrogen at 50 °C under 100 bar of H_2. The hydrogen storage capacity of TiVFeMgLi (3.50 g cm^{-3}) increases slightly from 2.31 wt% to 2.42 wt% hydrogen at 50 °C under 50 and 100 bar of H_2, respectively.

The recent progress of HEMs for hydrogen storage has been discussed in several reviews[235–237]. However, improving storage capacities by increasing H_2 pressure can lead to technological challenges and safety concerns during hydrogen storage and transportation (evaporation, embrittlement).

Photovoltaic HEMs

The HEM concept can be exploited to obtain photovoltaic materials with multifunctional profiles reconciling higher absorption coefficients, charge carrier concentrations, improved electron and hole mobilities, better carrier lifetimes and material longevity[238].

This can be achieved by compositional and structure-dependent bandgap design via elemental doping: by selecting suitable constituents and composition ratios, it is possible to engineer bandgaps suitable for absorbing wider portions of the electromagnetic spectrum. Compositional complexity can help to adjust the carrier mobility and concentration and allow incorporating a broader range of elements with different atomic sizes and electronic properties, potentially leading to improved electron and hole transport characteristics.

Following these ideas, several groups have tried to design multifunctional HEMs for solar cell applications, using metal oxides, sulfides, tellurides and selenides. These HEMs often use more than five or six different cations and anions, providing access to a large spectrum of crystal structures, bandgap ranges and carrier features, yet often with reduced material stability[239].

A multifunctional solar-selective absorbing high-entropy nitride coating was developed through computational guidance[240], optimizing conformational entropy and reactive magnetron sputtering methods. The synthesized AlCrTaTiZrN high-entropy nitride shows a combination of high solar absorption of 93.5% (as a reference, the solar absorption for an encapsulated standard c-Si photovoltaic cell is around 90%), a thermal emittance below 10%, a high photothermal conversion efficiency of 87.7% at 600 °C and good thermal stability, maintaining good optical properties even after annealing for 168 h in vacuum at 600 °C.

Non-toxic lead-free high-entropy perovskite halides with high absorption coefficients and good carrier lifetimes were also developed for optoelectronic devices[241]. These materials showed good colloidal stability, narrow band emission, high photoluminescence quantum yields and short fluorescence lifetimes, but decomposed into multiple phases.

Biologically active HEMs

Materials used in biomedical applications have to match multifunctional profiles. These include good mechanical properties (high yield strength, ductility, fatigue resistance, fracture toughness, bone-compatible Young's modulus) to withstand loads from physical activity and suppress bone decay; tribological and corrosion resistance to ensure durability in the human body and avoid infections that can be caused by abrasive material debris; biocompatibility to coexist with surrounding tissues; and thermal conduction coefficients that prevent proteinous synovial degeneration[242].

Biologically active HEMs have been studied since 2017 (refs. [242–249]). The entropy-driven phase stability and sluggish diffusion of such massive solid solutions slow down the formation and growth of structural defects. This can protect against fatigue damage and related gradual degradation effects when exposed to physiological environments for prolonged times[250]. Following these ideas, TiZrTaHfNb HEMs were designed[251] that show enhanced wear, corrosion resistance and mechanical performance compared with conventional load-bearing 316L, CoCrMo and Ti6Al4V alloys[242,252]. Alloy systems based on the hcp metals Ti, Zr and Hf blended with refractory bcc metals such as Nb, Ta or Mo have been studied widely in this context, mainly owing to their often low elastic modulus (when the resulting solid solution is in the bcc phase state), good strength and high corrosion resistance. The low Young's modulus of implants helps to avoid the stress-shielding effect that arises when the moduli of the implant and bone are very different under mechanical loading, which leads to unbalanced load sharing where the stiffer implant alloy takes up most

Review article

of the mechanical forces while the softer bone decays. A better stiffness balance can be realized when compositionally shifting such alloys into a (near-metastable) bcc phase field, in the vicinity of its transition back to the hcp structure. A possible shortcoming of such highly alloyed materials is their relatively high mass density relative to that of bone. This shows that in this field, a fine balance must be found between elastic modulus, biocompatibility, strength, wear, mass density and corrosion.

For biomedical applications, it is desirable to combine good antibacterial performance, high fracture toughness, low (bone-like) elastic stiffness (as a reference, the Young's modulus of cortical human bone is 17–25 GPa) and good fatigue resistance. This is a fundamental design challenge, as good antibacterial performance usually requires high amounts of Cu, which acts on bacteria via ion release. However, this element can also form unwanted intermetallic phases, causing galvanic corrosion and embrittlement[253]. A HEM that suppresses the formation of brittle phases even with higher amounts of Cu is an $Al_{0.4}CoCrCuFeNi$ HEM with a dual fcc phase structure[254], one rich in Cu (>22 at%) and the other rich in Co, Fe, Ni and Cr. Above >18 at% Cu, this material shows good antibacterial and mechanical performance.

Although most reported biomedical HEMs show enhanced mechanical performance compared with conventional materials, existing studies mainly focus on microstructural evolution and mechanical strength. Further research should target their in vivo biomedical properties.

Future perspectives

Among the many features of HEMs, perhaps the most pivotal is their seamless adjustability across a broad spectrum of chemical compositions. This characteristic holds promise for realizing properties that would otherwise be arduous to achieve or even unattainable. Noteworthy attributes accessible through the HEM concept encompass a high variability and complexity in electronic conductivity, chemically active surface sites, biocompatibility and enhanced magnetic moments, often paired with good mechanical properties.

Moreover, the microstructures of HEMs can be tailored through chemical adjustments, particularly through microstructure design routes that slightly deviate from the ideal solid solution yet are appealing and can be modulated through alloying and heat treatment. Attainable microstructure features include new multielement phases, spinodal decomposition, multiple order–disorder transitions, customized

chemical surfaces and chemically decorated defect states. These material states not only display new electronic, magnetic, transport and thermal properties but also allow their reconciliation with beneficial mechanical features, which establishes a more holistic design target for real-world applications with harsh mechanical loading and environmental conditions. Realizing both design paradigms within one HEM, with a blend of functional attributes minimally reliant on lattice defects and mechanical features and significantly influenced by microstructure, is thus a viable pathway for advanced multifunctional material design.

This approach offers avenues to realize materials with interesting functional properties, such as specific thermal expansion or effective catalytic sites, combined with additional properties, integrating contrasting or effects previously deemed incompatible. This is important, as the use of real-world materials is not confined to a solitary property dimension but frequently requires fulfilling a spectrum of conflicting properties, and enhancing one (for example, high strength) typically triggers a decline in another (for example, soft magnetic properties).

A sometimes overlooked facet in the HEM field is concerns associated with sustainability, CO_2 balance and costs[255,256] (Fig. 6). Numerous compositionally complex materials possess alluring properties that can rival those of established commercial materials. However, these materials often lack competitiveness in their sustainability, responsible production and pricing. This point has not yet been sufficiently reflected in the literature. Another pressing issue is recyclability, which is expected to be increasingly challenging owing to the increasing chemical complexity of HEMs.

Many elements ideally suited for multifunctional, chemically complex materials suffer from limited availability, severe environmental repercussions, or exceedingly high and volatile market values. Therefore, it becomes imperative to target the development of multifunctional HEMs that are both more performant and more sustainable than established materials. Applications requiring minimal volumes are particularly interesting even when reliant on critical and less sustainable alloy constituents: these include catalysts, protective thin coatings, magnets, low thermal expansion alloys and functional wires.

Another interesting possibility is to widen HEM design from the bulk to defects (dislocations, interfaces, surfaces and so on). For some applications, specific properties can be achieved by tuning the chemical composition of the defects and not of the entire bulk material,


Energy footprint 0 – 560 MJ kg⁻¹ | Carbon footprint 0 – 40 CO₂-eq kg⁻¹ | Price 0 – 150 € kg⁻¹
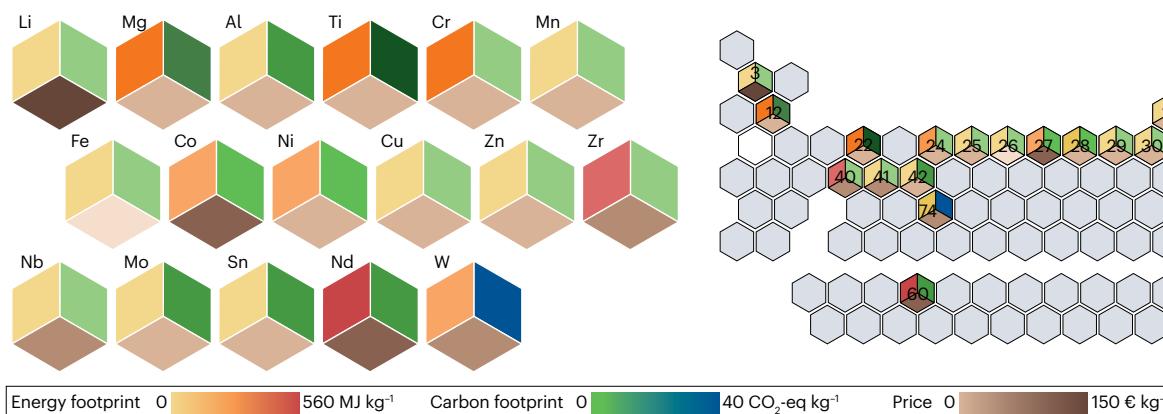
Fig. 6 | Sustainability and cost considerations for high-entropy materials. Aspects such as sustainability, responsible use of elements, absolute price and cost variations need to be considered when designing new high-entropy materials (HEMs): new multifunctional materials that aim to surpass existing ones must also offer better performance in these categories and not just in the functional and mechanical properties. The figure shows the huge differences in these properties among typical HEM alloying elements. Data from ref. 261 and http://www.leonland.de/elements_by_price/list.

Review article

in which expensive alloying elements can get 'lost' by dilution. Such a lattice defect-oriented HEM development can be guided by the Gibbs adsorption isotherm, that is, by using elements with a high tendency to segregate to interfaces, surfaces or dislocations, together with other segregating elements. In this way, the chemical complexity of the defects and their functionalization can be promoted over that of the bulk. For such a design strategy, it is not the elements with the highest but those with the lowest solubility in the bulk solid solution that are interesting (additional) alloy candidates because they usually have a high segregation trend to lattice defects. This means that elements with high bulk solubility must be chosen to stabilize a massive solid solution matrix and those with low solubility must be additionally blended to form high-entropy lattice defects. The entropy-driven design principle is then turned upside down, because elements with a high segregation trend to interfaces usually have a low solubility in the bulk and vice versa. Such a design principle might open up new opportunities for more sustainable functional interface and dislocation design by using chemical complexity only where needed and not throughout the entire bulk material. Specific target materials might be catalysts, multifunctional coatings, and materials resistant to corrosion, fatigue and hydrogen intrusion.

Another avenue for material exploration lies in widening the scope from the current four-element to five-element HEMs to a wider range of materials and alloying elements, including interstitials (such as C, N, H, B and O). As an example, many possible HEMs with six, seven and even eight alloying elements have been suggested[63] by combining text mining along a 'chemical similarity index' with physics-based descriptor filtering of the results. In general, owing to the practically infinite compositional and microstructural space of HEMs, it is essential to include (combined) methods from artificial intelligence based on text mining, active learning and graph theory into the (high-throughput) material development, in concert with existing thermodynamic and kinetic databases[257–259].

References

1. Yeh, J. W. et al. Nanostructured high-entropy alloys with multiple principal elements: novel alloy design concepts and outcomes. *Adv. Eng. Mater.* **6**, 299–303 (2004).
2. Yeh, J.-W. in *High-Entropy Alloys: Fundamentals and Applications* (eds Gao, M. C. et al.) 1–19 (Springer, 2016).
3. Murty, B. S., Yeh, J. W., Ranganathan, S. & A brief history of alloys and the birth of high-entropy alloys. *High Entropy Alloys* https://doi.org/10.1016/b978-0-12-800251-3.00001-8 (2014).
4. Cantor, B. Multicomponent and high entropy alloys. *Entropy* **16**, 4749–4768 (2014).
5. George, E. P., Raabe, D. & Ritchie, R. O. High-entropy alloys. *Nat. Rev. Mater.* **4**, 515–534 (2019).
6. Tsai, M. H. Physical properties of high entropy alloys. *Entropy* **15**, 5338–5345 (2013).
7. Senkov, O. N., Wilks, G. B., Miracle, D. B., Chuang, C. P. & Liaw, P. K. Refractory high-entropy alloys. *Intermetallics* **18**, 1758–1765 (2010).
8. Zhang, Y., Yang, X. & Liaw, P. K. Alloy design and properties optimization of high-entropy alloys. *JOM* **64**, 830–838 (2012).
9. Li, Z., Pradeep, K. G., Deng, Y., Raabe, D. & Tasan, C. C. Metastable high-entropy dual-phase alloys overcome the strength–ductility trade-off. *Nature* **534**, 227–30 (2016).
10. Zhang, Y. et al. Microstructures and properties of high-entropy alloys. *Prog. Mater. Sci.* **61**, 1–93 (2014).
11. Li, Z. & Raabe, D. Strong and ductile non-equiatomic high-entropy alloys: design, processing, microstructure, and mechanical properties. *JOM* **69**, 2099–2106 (2017).
12. Li, Z. Interstitial equiatomic CoCrFeMnNi high-entropy alloys: carbon content, microstructure, and compositional homogeneity effects on deformation behavior. *Acta Mater.* **164**, 400–412 (2019).
13. Gludovatz, B., George, E. P. & Ritchie, R. O. Processing, microstructure and mechanical properties of the CrMnFeCoNi high-entropy alloy. *JOM* **67**, 2262–2270 (2015).
14. Lu, W. et al. Interfacial nanophases stabilize nanotwins in high-entropy alloys. *Acta Mater.* **185**, 218–232 (2019).
15. Li, L. et al. Segregation-driven grain boundary spinodal decomposition as a pathway for phase nucleation in a high-entropy alloy. *Acta Mater.* **178**, 1–9 (2019).
16. Donohue, M. D. & Aranovich, G. L. Classification of Gibbs adsorption isotherms. *Adv. Colloid Interface Sci.* **76–77**, 137–152 (1998).
17. McLean, D. & Maradudin, A. Grain boundaries in metals. *Phys. Today* **11**, 35–36 (1958).
18. Li, L., Kamachali, R. D., Li, Z. & Zhang, Z. Grain boundary energy effect on grain boundary segregation in an equiatomic high-entropy alloy. *Phys. Rev. Mater.* **4**, 53603 (2020).
19. Korte-Kerzel, S. et al. Defect phases — thermodynamics and impact on material properties. *Int. Mater. Rev.* **67**, 89–117 (2022).
20. Welk, B. A. et al. Nature of the interfaces between the constituent phases in the high entropy alloy CoCrCuFeNiAl. *Ultramicroscopy* **134**, 193–199 (2013).
21. Ghigna, P. et al. Lithiation mechanism in high-entropy oxides as anode materials for Li-ion batteries: an operando XAS study. *ACS Appl. Mater. Interfaces* **12**, 50344–50354 (2020).
22. Schneeweiss, O. et al. Magnetic properties of the CrMnFeCoNi high-entropy alloy. *Phys. Rev. B* **96**, 014437 (2017).
23. Pickering, E. J. & Jones, N. G. High-entropy alloys: a critical assessment of their founding principles and future prospects. *Int. Mater. Rev.* **61**, 183–202 (2016).
24. Mu, S., Pei, Z., Liu, X. & Stocks, G. M. Electronic transport and phonon properties of maximally disordered alloys: from binaries to high-entropy alloys. *J. Mater. Res.* **33**, 2857–2880 (2018).
25. Rao, Z. et al. Unveiling the mechanism of abnormal magnetic behavior of FeNiCoMnCu high-entropy alloys through a joint experimental-theoretical study. *Phys. Rev. Mater.* **4**, 14402 (2020).
26. Gao, M. C. et al. High-entropy functional materials. *J. Mater. Res.* **33**, 3138–3155 (2018).
27. Yeh, J.-W., Chen, S. K., Shih, H. C., Zhang, Y. & Zuo, T. T. in *High-Entropy Alloys: Fundamentals and Applications* (eds Gao, M. C. et al.) 237–265 (Springer, 2016).
28. Duan, J. et al. A novel high-entropy alloy with an exceptional combination of soft magnetic properties and corrosion resistance. *Sci. China Mater.* **66**, 772–779 (2023).
29. Mishra, R. K., Sahay, P. P. & Shahi, R. R. Alloying, magnetic and corrosion behavior of AlCrFeMnNiTi high entropy alloy. *J. Mater. Sci.* **54**, 4433–4443 (2019).
30. Jin, X. et al. CoCrFeMnNi high-entropy alloy powder with excellent corrosion resistance and soft magnetic property prepared by gas atomization method. *Materwiss. Werkstofftech.* **50**, 837–843 (2019).
31. Wang, W. et al. A corrosion-resistant soft-magnetic high entropy alloy. *Mater. Lett.* **304**, 130571 (2021).
32. Zhang, H. et al. A novel FeCoNiCr$_{0.2}$Si$_{0.2}$ high entropy alloy with an excellent balance of mechanical and soft magnetic properties. *J. Magn. Magn. Mater.* **478**, 116–121 (2019).
33. Chen, C. et al. A novel ultrafine-grained high entropy alloy with excellent combination of mechanical and soft magnetic properties. *J. Magn. Magn. Mater.* **502**, 166513 (2020).
34. Liu, X. & Vecchio, K. Simultaneously improving mechanical and magnetic properties through heterogeneous lamella structures in a superalloy-like, soft magnetic complex concentrated alloy. *Mater. Res. Lett.* **11**, 749–756 (2023).
35. Fu, Z. et al. Exceptional combination of soft magnetic and mechanical properties in a heterostructured high-entropy composite. *Appl. Mater. Today* **15**, 590–598 (2019).
36. Li, Z. et al. Strength, plasticity and coercivity tradeoff in soft magnetic high-entropy alloys by multiple coherent interfaces. *Acta Mater.* **254**, 118970 (2023).
37. Han, L. et al. A mechanically strong and ductile soft magnet with extremely low coercivity. *Nature* **608**, 310–316 (2022).
38. Han, L. et al. Ultrastrong and ductile soft magnetic high-entropy alloys via coherent ordered nanoprecipitates. *Adv. Mater.* **33**, 2102139 (2021).
39. Han, L. et al. Strong and ductile high temperature soft magnets through Widmanstätten precipitates. *Nat. Commun.* **14**, 8176 (2023).
40. Nemani, S. K., Torkamanzadeh, M., Wyatt, B. C., Presser, V. & Anasori, B. Functional two-dimensional high-entropy materials. *Commun. Mater.* **4**, 16 (2023).
41. Löffler, T., Ludwig, A., Rossmeisl, J. & Schuhmann, W. What makes high-entropy alloys exceptional electrocatalysts? *Angew. Chem. Int. Ed.* **60**, 26894–26903 (2021).
42. Tomboc, G. M., Kwon, T., Joo, J. & Lee, K. High entropy alloy electrocatalysts: a critical assessment of fabrication and performance. *J. Mater. Chem. A Mater.* **8**, 14844–14862 (2020).
43. Banko, L. et al. Unravelling composition–activity–stability trends in high entropy alloy electrocatalysts by using a data-guided combinatorial synthesis strategy and computational modeling. *Adv. Energy Mater.* **12**, 2103312 (2022).
44. Luo, H., Li, Z. & Raabe, D. Hydrogen enhances strength and ductility of an equiatomic high-entropy alloy. *Sci. Rep.* **7**, 9892 (2017).
45. Luo, H., Li, Z., Mingers, A. M. & Raabe, D. Corrosion behavior of an equiatomic CoCrFeMnNi high-entropy alloy compared with 304 stainless steel in sulfuric acid solution. *Corros. Sci.* **134**, 131–139 (2018).
46. Luo, H. et al. A strong and ductile medium-entropy alloy resists hydrogen embrittlement and corrosion. *Nat. Commun.* **11**, 3081 (2020).
47. Körmann, F. et al. 'Treasure maps' for magnetic high-entropy-alloys from theory and experiment. *Appl. Phys. Lett.* **107**, 142404 (2015).
48. Lucas, M. S. et al. Magnetic and vibrational properties of high-entropy alloys. *J. Appl. Phys.* **109**, 10–13 (2011).
49. Liu, X., Zhang, J. & Pei, Z. Machine learning for high-entropy alloys: progress, challenges and opportunities. *Prog. Mater. Sci.* **131**, 101018 (2023).
50. Rickman, J. M., Balasubramanian, G., Marvel, C. J., Chan, H. M. & Burton, M.-T. Machine learning strategies for high-entropy alloys. *J. Appl. Phys.* **128**, 221101 (2020).
51. Raabe, D., Mianroodi, J. R. & Neugebauer, J. Accelerating the design of compositionally complex materials via physics-informed artificial intelligence. *Nat. Comput. Sci.* **3**, 198–209 (2023).

Review article

52. Pei, Z., Yin, J., Hawk, J. A., Alman, D. E. & Gao, M. C. Machine-learning informed prediction of high-entropy solid solution formation: beyond the Hume–Rothery rules. *NPJ Comput. Mater.* **6**, 50 (2020).

53. Qiao, L., Liu, Y. & Zhu, J. A focused review on machine learning aided high-throughput methods in high entropy alloy. *J. Alloy. Compd.* **877**, 160295 (2021).

54. Ma, D., Grabowski, B., Körmann, F., Neugebauer, J. & Raabe, D. Ab initio thermodynamics of the CoCrFeMnNi high entropy alloy: importance of entropy contributions beyond the configurational one. *Acta Mater.* **100**, 90–97 (2015).

55. Zhang, F. et al. An understanding of high entropy alloys from phase diagram calculations. *CALPHAD* **45**, 1–10 (2014).

56. Curtarolo, S. et al. The high-throughput highway to computational materials design. *Nat. Mater.* **12**, 191–201 (2013).

57. Holm, E. A. et al. Overview: computer vision and machine learning for microstructural characterization and analysis. *Metall. Mater. Trans. A* **51**, 5985–5999 (2020).

58. Muhammad, W., Brahme, A. P., Ibragimova, O., Kang, J. & Inal, K. A machine learning framework to predict local strain distribution and the evolution of plastic anisotropy & fracture in additively manufactured alloys. *Int. J. Plast.* **136**, 102867 (2021).

59. Yang, Z. et al. Establishing structure–property localization linkages for elastic deformation of three-dimensional high contrast composites using deep learning approaches. *Acta Mater.* **166**, 335–345 (2019).

60. Raabe, D. et al. Current challenges and opportunities in microstructure-related properties of advanced high-strength steels. *Metall. Mater. Trans. A* **51**, 5517–5586 (2020).

61. Halpren, E., Yao, X., Chen, Z. W. & Singh, C. V. Machine learning assisted design of BCC high entropy alloys for room temperature hydrogen storage. *Acta Mater.* **270**, 119841 (2024).

62. Sasidhar, K. N. et al. Enhancing corrosion-resistant alloy design through natural language processing and deep learning. *Sci. Adv.* **9**, 7992 (2023).

63. Pei, Z., Yin, J., Liaw, P. K. & Raabe, D. Toward the design of ultrahigh-entropy alloys via mining six million texts. *Nat. Commun.* **14**, 54 (2023).

64. Sandlöbes, S. et al. A rare-earth free magnesium alloy with improved intrinsic ductility. *Sci. Rep.* **7**, 10458 (2017).

65. Zhao, S. et al. Machine learning assisted design of high-entropy alloys with ultra-high microhardness and unexpected low density. *Mater. Des.* https://doi.org/10.1016/j.matdes.2024.112634 (2024).

66. Rao, Z. et al. Machine learning–enabled high-entropy alloy discovery. *Science* **378**, 78–85 (2022).

67. Katiyar, N. K., Goel, G. & Goel, S. Emergence of machine learning in the development of high entropy alloy and their prospects in advanced engineering applications. *Emergent Mater.* **4**, 1635–1648 (2021).

68. Bauer, S. et al. Roadmap on data-centric materials science. *Model. Simul. Mater. Sci. Eng.* **32**, 063301 (2024).

69. Shi, L. et al. Connecting the composition, structure, and magnetic property in high-entropy metallic glasses. *Acta Mater.* **254**, 118983 (2023).

70. Pedersen, J. K. et al. Bayesian optimization of high-entropy alloy compositions for electrocatalytic oxygen reduction. *Angew. Chem. Int. Ed.* **60**, 24144–24152 (2021).

71. Khatamsaz, D. et al. Bayesian optimization with active learning of design constraints using an entropy-based approach. *NPJ Comput. Mater.* **9**, 49 (2023).

72. Kim, M. et al. Exploring optimal water splitting bifunctional alloy catalyst by pareto active learning. *Adv. Mater.* **35**, 2211497 (2023).

73. Sathiyamoorthi, P. & Kim, H. S. High-entropy alloys with heterogeneous microstructure: processing and mechanical properties. *Prog. Mater. Sci.* **123**, 100709 (2022).

74. Chen, T. et al. Microstructure and properties of TiC/Fe$_{24}$Ni$_{24}$Co$_{24}$Mn$_{18}$ high-entropy composite with exceptionally low coercivity. *Mater. Today Commun.* **35**, 106150 (2023).

75. Ferrari, A., Körmann, F., Asta, M. & Neugebauer, J. Simulating short-range order in compositionally complex materials. *Nat. Comput. Sci.* **3**, 221–229 (2023).

76. Zhang, Y., Zuo, T., Cheng, Y. & Liaw, P. K. High-entropy alloys with high saturation magnetization, electrical resistivity, and malleability. *Sci. Rep.* **3**, 1455 (2013).

77. Yan, X. & Zhang, Y. Functional properties and promising applications of high entropy alloys. *Scr. Mater.* **187**, 188–193 (2020).

78. Chaudhary, V., Chaudhary, R., Banerjee, R. & Ramanujan, R. V. Accelerated and conventional development of magnetic high entropy alloys. *Mater. Today* **49**, 231–252 (2021).

79. Xu, J., Zhao, Z. F. & Wang, Y. Effect of annealing treatment on the microstructure and magnetic properties of FeSiBAlNi (C, Ce) high entropy alloys. *Mater. Sci. Forum* **849**, 52–57 (2016).

80. Morley, N. A., Lim, B., Xi, J., Quintana-Nedelcos, A. & Leong, Z. Magnetic properties of the complex concentrated alloy system CoFeNi$_{0.5}$Cr$_{0.5}$Al$_x$. *Sci. Rep.* **10**, 14506 (2020).

81. Cieslak, J., Tobola, J. & Reissner, M. The effect of bcc/fcc phase preference on magnetic properties of Al$_x$CrFeCoNi high entropy alloys. *Intermetallics* **118**, 106672 (2020).

82. Zhou, K. X. et al. FeCoNiAlSi high entropy alloys with exceptional fundamental and application-oriented magnetism. *Intermetallics* **122**, 106801 (2020).

83. Sahu, P., Bagri, A. S., Anoop, M. D., Kumar, M. & Kumar, V. Impact of Si and Mg on microstructural and magnetic behavior of Fe–Co–Ni (Mg–Si)x (x=0.00,0.1,0.2) multicomponent alloys. *Silicon* **12**, 893–902 (2020).

84. Borkar, T. et al. A combinatorial approach for assessing the magnetic properties of high entropy alloys: role of Cr in AlCo$_x$Cr$_{1-x}$FeNi. *Adv. Eng. Mater.* **19**, 1700048 (2017).

85. Zhang, Q. et al. The effects of phase constitution on magnetic and mechanical properties of FeCoNi(CuAl)$_x$ (x=0–1.2) high-entropy alloys. *J. Alloy. Compd.* **693**, 1061–1067 (2017).

86. Mishra, R. K. & Shahi, R. R. Phase evolution and magnetic characteristics of TiFeNiCr and TiFeNiCrM (M=Mn, Co) high entropy alloys. *J. Magn. Magn. Mater.* **442**, 218–223 (2017).

87. Huang, S., Vida, Á., Heczel, A., Holmström, E. & Vitos, L. Thermal expansion, elastic and magnetic properties of FeCoNiCu-based high-entropy alloys using first-principle theory. *JOM* **69**, 2107–2112 (2017).

88. Zhang, X., Han, L., Dehm, G. & Liebscher, C. H. Microstructure and physical properties of dual-phase soft magnetic Fe–Co–Ti–Ge alloys. *J. Alloy. Compd.* **945**, 169282 (2023).

89. Kurniawan, M., Perrin, A., Xu, P., Keylin, V. & McHenry, M. Curie temperature engineering in high entropy alloys for magnetocaloric applications. *IEEE Magn. Lett.* **7**, 1–5 (2016).

90. Zhang, B. et al. Magnetic transformation of Mn from anti-ferromagnetism to ferromagnetism in FeCoNiZMn$_x$ (Z = Si, Al, Sn, Ge) high entropy alloys. *J. Mater. Sci. Technol.* **68**, 124–131 (2021).

91. Zuo, T. et al. Tailoring magnetic behavior of CoFeMnNiX (X = Al, Cr, Ga, and Sn) high entropy alloys by metal doping. *Acta Mater.* **130**, 10–18 (2017).

92. Herzer, G. Grain size dependence of coercivity and permeability in nanocrystalline ferromagnets. *IEEE Trans. Magn.* **26**, 1397–1402 (1990).

93. Pavithra, C. L. P. et al. An advancement in the synthesis of unique soft magnetic CoCuFeNiZn high entropy alloy thin films. *Sci. Rep.* **11**, 8836 (2021).

94. Zhang, Y., Zuo, T., Cheng, Y. & Liaw, P. K. High-entropy alloys with high saturation magnetization, electrical resistivity and malleability. *Sci. Rep.* **3**, 1455 (2013).

95. Song, X., Liaw, P. K., Wei, Z., Liu, Z. & Zhang, Y. Evolution of the microstructures, magnetic and mechanical behaviors of Co$_{47.5}$Fe$_{28.5}$Ni$_{19}$Si$_{3.4}$Al$_{1.6}$ high-entropy alloy fabricated by laser powder bed fusion. *Addit. Manuf.* **71**, 103593 (2023).

96. Coey, J. M. D. *Magnetism and Magnetic Materials* (Cambridge Univ. Press, 2010).

97. Kuz'min, M. D., Skokov, K. P., Jian, H., Radulov, I. & Gutfleisch, O. Towards high-performance permanent magnets without rare earths. *J. Phys. Condens. Matter* **26**, 064205 (2014).

98. Gao, Q., Opahle, I., Gutfleisch, O. & Zhang, H. Designing rare-earth free permanent magnets in Heusler alloys via interstitial doping. *Acta Mater.* **186**, 355–362 (2020).

99. Na, S.-M., Lambert, P. K. & Jones, N. J. Hard magnetic properties of FeCoNiAlCu$_x$Ti$_x$ based high entropy alloys. *AIP Adv.* **11**, 015210 (2021).

100. Chen, H., Gou, J., Jia, W., Song, X. & Ma, T. Origin of hard magnetism in Fe–Co–Ni–Al–Ti–Cu high-entropy alloy: chemical shape anisotropy. *Acta Mater.* **246**, 118702 (2023).

101. Lan, Q. et al. Highly tunable magnetic behavior resulting from hierarchical phase separation in AlCo(Cr)FeNi high-entropy alloys. *iScience* **25**, 104047 (2022).

102. Dasari, S. et al. Highly tunable magnetic and mechanical properties in an Al$_{0.3}$CoFeNi complex concentrated alloy. *Materialia* **12**, 100755 (2020).

103. Kovács, A. et al. Role of heterophase interfaces on local coercivity mechanisms in the magnetic Al$_{0.3}$CoFeNi complex concentrated alloy. *Acta Mater.* **246**, 118672 (2023).

104. Vishina, A. et al. High-throughput and data-mining approach to predict new rare-earth free permanent magnets. *Phys. Rev. B* **101**, 94407 (2020).

105. Xia, W. et al. Accelerating the discovery of novel magnetic materials using machine learning–guided adaptive feedback. *Proc. Natl Acad. Sci. USA* **119**, e2204485119 (2022).

106. Hirayama, Y., Takahashi, Y. K., Hirosawa, S. & Hono, K. Intrinsic hard magnetic properties of Sm(Fe$_{1-x}$Co$_x$)$_{12}$ compound with the ThMn$_{12}$ structure. *Scr. Mater.* **138**, 62–65 (2017).

107. Tozman, P., Sepehri-Amin, H., Takahashi, Y. K., Hirosawa, S. & Hono, K. Intrinsic magnetic properties of Sm(Fe$_{1-x}$Co$_x$)$_{11}$Ti and Zr-substituted Sm$_{1-y}$Zr$_y$(Fe$_{0.8}$Co$_{0.2}$)$_{11.5}$Ti$_{0.5}$ compounds with ThMn$_{12}$ structure toward the development of permanent magnets. *Acta Mater.* **153**, 354–363 (2018).

108. Tozman, P., Sepehri-Amin, H. & Hono, K. Prospects for the development of SmFe$_{12}$-based permanent magnets with a ThMn$_{12}$-type phase. *Scr. Mater.* **194**, 113686 (2021).

109. Nguyen, D.-N., Kino, H., Miyake, T. & Dam, H.-C. Explainable active learning in investigating structure–stability of SmFe$_{12-\alpha-\beta}$X$_\alpha$Y$_\beta$ structures X, Y {Mo, Zn, Co, Cu, Ti, Al, Ga}. *MRS Bull.* **48**, 31–44 (2023).

110. Fukazawa, T., Harashima, Y., Hou, Z. & Miyake, T. Bayesian optimization of chemical composition: a comprehensive framework and its application to R Fe$_{12}$-type magnet compounds. *Phys. Rev. Mater.* **3**, 053807 (2019).

111. Gutfleisch, O. et al. Mastering hysteresis in magnetocaloric materials. *Phil. Trans. R. Soc. A* **374**, 20150308 (2016).

112. Scheibel, F. et al. Hysteresis design of magnetocaloric materials — from basic mechanisms to applications. *Energy Technol.* **6**, 1397–1428 (2018).

113. Gottschall, T. et al. Making a cool choice: the materials library of magnetic refrigeration. *Adv. Energy Mater.* **9**, 1901322 (2019).

114. Tegus, O., Brück, E., Buschow, K. H. J. & de Boer, F. R. Transition-metal-based magnetic refrigerants for room-temperature applications. *Nature* **415**, 150–152 (2002).

115. Fries, M. et al. Microstructural and magnetic properties of Mn–Fe–P–Si (Fe$_2$ P-type) magnetocaloric compounds. *Acta Mater.* **132**, 222–229 (2017).

116. Lu, S. F. et al. Effect of configuration entropy on magnetocaloric effect of rare earth high-entropy alloy. *J. Alloy. Compd.* **874**, 159918 (2021).

117. Lu, S. F. et al. Magnetocaloric effect of high-entropy rare-earth alloy GdTbHoErY. *J. Mater. Sci. Mater. Electron.* **32**, 10919–10926 (2021).

118. Yuan, Y. et al. Rare-earth high-entropy alloys with giant magnetocaloric effect. *Acta Mater.* **125**, 481–489 (2017).

119. Guo, D., Moreno-Ramírez, L. M., Law, J.-Y., Zhang, Y. & Franco, V. Excellent cryogenic magnetocaloric properties in heavy rare-earth based HRENiGa$_2$ (HRE = Dy, Ho, or Er) compounds. *Sci. China Mater.* **66**, 249–256 (2023).

120. Dong, Z. et al. Mn$_x$Cr$_{0.3}$Fe$_{0.5}$Co$_{0.2}$Ni$_{0.5}$Al$_{0.3}$ high entropy alloys for magnetocaloric refrigeration near room temperature. *J. Mater. Sci. Technol.* **79**, 15–20 (2021).

Review article

121. Dong, Z., Wang, Z. & Yin, S. Magnetic properties and large cryogenic magneto-caloric effect of $Er_{0.2}Tm_{0.2}Ho_{0.2}Cu_{0.2}Co_{0.2}$ amorphous ribbon. *Intermetallics* **124**, 106879 (2020).

122. Zhang, Y. et al. Tunable magnetic phase transition and magnetocaloric effect in the rare-earth-free Al–Mn–Fe–Co–Cr high-entropy alloys. *Mater. Des.* **229**, 111894 (2023).

123. Zhang, Y. The emergence of considerable room temperature magnetocaloric performances in the transition metal high-entropy alloys. *Mater. Today Phys.* **32**, 101031 (2023).

124. Zhang, F. et al. Impact of fast-solidification on all-*d*-metal NiCoMnTi based giant magnetocaloric Heusler compounds. *Acta Mater.* **265**, 119595 (2024).

125. Law, J. Y. & Franco, V. Review on magnetocaloric high-entropy alloys: design and analysis methods. *J. Mater. Res.* **38**, 37–51 (2023).

126. Law, J. Y., Díaz-García, Á., Moreno-Ramírez, L. M. & Franco, V. Increased magnetocaloric response of FeMnNiGeSi high-entropy alloys. *Acta Mater.* **212**, 116931 (2021).

127. Taubel, A. et al. Tailoring magnetocaloric effect in all-*d*-metal Ni-Co-Mn-Ti Heusler alloys: a combined experimental and theoretical study. *Acta Mater.* **201**, 425–434 (2020).

128. Beckmann, B. et al. Dissipation losses limiting first-order phase transition materials in cryogenic caloric cooling: a case study on all-*d*-metal Ni(–Co)–Mn–Ti Heusler alloys. *Acta Mater.* **246**, 118695 (2023).

129. Khan, A. N., Díaz-García, Á., Moreno-Ramírez, L. M., Law, J. Y. & Franco, V. Tunable magnetocaloric effect towards cryogenic range by varying Mn:Ni ratio in all-*d*-metal Ni(Co)–Mn–Ti Heusler alloys. *J. Alloy. Compd.* **973**, 172938 (2024).

130. Taubel, A. et al. Influence of magnetic field, chemical pressure and hydrostatic pressure on the structural and magnetocaloric properties of the Mn–Ni–Ge system. *J. Phys. D* **50**, 464005 (2017).

131. Fortunato, N. M. et al. High-throughput design of magnetocaloric materials for energy applications: MM'X alloys. *Adv. Sci.* **10**, 2206772 (2023).

132. Rowe, D. M. *CRC Handbook of Thermoelectrics* (CRC Press, 2018).

133. Snyder, G. J. & Toberer, E. S. Complex thermoelectric materials. *Nat. Mater.* **7**, 105–114 (2008).

134. Liu, D., Qin, B. & Zhao, L.-D. SnSe/SnS: multifunctions beyond thermoelectricity. *Mater. Lab.* **1**, 220006 (2022).

135. He, R. et al. Studies on mechanical properties of thermoelectric materials by nanoindentation. *Phys. Status Solidi* **212**, 2191–2195 (2015).

136. Rogl, G. et al. Mechanical properties of half-Heusler alloys. *Acta Mater.* **107**, 178–195 (2016).

137. Liu, Z. et al. Mechanical properties of nanostructured thermoelectric materials α-MgAgSb. *Scr. Mater.* **127**, 72–75 (2017).

138. Xia, X. et al. High-temperature oxidation behavior of filled skutterudites $YbyCo_4Sb_{12}$. *J. Electron. Mater.* **41**, 2225–2231 (2012).

139. Li, F., Wei, T. R., Kang, F. & Li, J. F. Thermal stability and oxidation resistance of BiCuSeO based thermoelectric ceramics. *J. Alloy. Compd.* **614**, 394–400 (2014).

140. Zhu, Y.-K. et al. Mediating point defects endows n-type Bi_2Te_3 with high thermoelectric performance and superior mechanical robustness for power generation application. *Small* **18**, 2201352 (2022).

141. Ge, Z.-H. et al. Low-cost, abundant binary sulfides as promising thermoelectric materials. *Mater. Today* **19**, 227–239 (2016).

142. Zhang, J. et al. Discovery of high-performance low-cost n-type Mg_3Sb_2-based thermoelectric materials with multi-valley conduction bands. *Nat. Commun.* **8**, 13901 (2017).

143. Perumal, S., Roychowdhury, S., Negi, D. S., Datta, R. & Biswas, K. High thermoelectric performance and enhanced mechanical stability of p-type $Ge_{1-x}Sb_xTe$. *Chem. Mater.* **27**, 7171–7178 (2015).

144. Hatzikraniotis, E., Zorbas, K. T., Samaras, I., Kyratsi, T. & Paraskevopoulos, K. M. Efficiency study of a commercial thermoelectric power generator (TEG) under thermal cycling. *J. Electron. Mater.* **39**, 2112–2116 (2010).

145. Al-Merbati, A. S., Yilbas, B. S. & Sahin, A. Z. A model study for cyclic thermal loading and thermal performance of a thermoelectric generator. *Int. J. Energy Res.* **38**, 1351–1360 (2014).

146. Dong, J., Gao, J. & Yan, Q. High entropy strategy on thermoelectric materials. *Mater. Lab.* **2**, 230001 (2023).

147. Jiang, B. et al. High figure-of-merit and power generation in high-entropy GeTe-based thermoelectrics. *Science* **377**, 208–213 (2022).

148. Jiang, F. et al. Structure, magnetic and thermoelectric properties of high entropy selenides $Bi_{0.6}Sb_{0.6}In_{0.4}Cr_{0.4}Se_3$. *Mater. Lab.* **1**, 220045 (2022).

149. Ma, Z. et al. High thermoelectric performance and low lattice thermal conductivity in lattice-distorted high-entropy semiconductors $AgMnSn_{1-x}Pb_xSbTe_4$. *Chem. Mater.* **34**, 8959–8967 (2022).

150. Kumar, A., Dragoe, D., Berardan, D. & Dragoe, N. Thermoelectric properties of high-entropy rare-earth cobaltates. *J. Materiomics* **9**, 191–196 (2023).

151. Zhang, P. et al. High-entropy $(Ca_{0.2}Sr_{0.2}Ba_{0.2}La_{0.2}Pb_{0.2})TiO_3$ perovskite ceramics with A-site short-range disorder for thermoelectric applications. *J. Mater. Sci. Technol.* **97**, 182–189 (2022).

152. Lou, Z. et al. A novel high-entropy perovskite ceramics $Sr_{0.9}La_{0.1}(Zr_{0.25}Sn_{0.25}Ti_{0.25}Hf_{0.25})O_3$ with low thermal conductivity and high Seebeck coefficient. *J. Eur. Ceram. Soc.* **42**, 3480–3488 (2022).

153. Zhang, Z. et al. Entropy engineering induced exceptional thermoelectric and mechanical performances in $Cu_{2-y}Ag_yTe_{1-2x}Se_xSe_x$. *Acta Mater.* **224**, 117512 (2022).

154. Chen, R. et al. Entropy-driven multiscale defects enhance the thermoelectric properties of ZrCoSb-based half-Heusler alloys. *Chem. Eng. J.* **455**, 140676 (2023).

155. Jiang, B. et al. High-entropy-stabilized chalcogenides with high thermoelectric performance. *Science* **371**, 830–834 (2021).

156. Shafeie, S. et al. High-entropy alloys as high-temperature thermoelectric materials. *J. Appl. Phys.* **118**, 184905 (2015).

157. Pei, Y. et al. Convergence of electronic bands for high performance bulk thermoelectrics. *Nature* **473**, 66–69 (2011).

158. Wang, X. et al. Enhanced thermoelectric performance in high entropy alloys $Sn_{0.25}Pb_{0.25}Mn_{0.25}Ge_{0.25}Te$. *ACS Appl. Mater. Interfaces* **13**, 18638–18647 (2021).

159. Liu, R. et al. Entropy as a gene-like performance indicator promoting thermoelectric materials. *Adv. Mater.* **29**, 1702712 (2017).

160. Roychowdhury, S. et al. Enhanced atomic ordering leads to high thermoelectric performance in $AgSbTe_2$. *Science* **371**, 722–727 (2021).

161. Campbell, F. C. *Elements of Metallurgy and Engineering Alloys* (ASM International, 2008).

162. Wassermann, E. F. & Acet, M. in *Magnetism and Structure in Functional Materials* (eds Planes, A. et al.) 177–197 (Springer, 2005).

163. Rao, Z. et al. 3*d* transition-metal high-entropy Invar alloy developed by adjusting the valence-electron concentration. *Phys. Rev. Mater.* **5**, 044406 (2021).

164. Rao, Z., Springer, H., Ponge, D. & Li, Z. Combinatorial development of multicomponent Invar alloys via rapid alloy prototyping. *Materialia* **21**, 101326 (2022).

165. Acet, M. Inducing strong magnetism in $Cr_{20}Mn_{20}Fe_{20}Co_{20}Ni_{20}$ high-entropy alloys by exploiting its anti-Invar property. *AIP Adv.* **9**, 095037 (2019).

166. Masumoto, H. On the thermal expansion of alloys of cobalt iron and chromium and a new alloy 'stainless invar'. *Sci. Report. Tohoku. Imp. Univ.* **23**, 265–275 (1934).

167. Masumoto, H. On the thermal expansion of the alloys of iron, nickel, and cobalt and the cause of the small expansibility of the alloys of the Invar type. *Sci. Rep. Tohoku Imp. Univ.* **20**, 101–123 (1931).

168. Orbay, Y. et al. Magnetic properties of the FCC and BCC phases of $(MnFeCoNi)_{80}Cu_{20-x}Z_x$ (Z: Al, Ga) high-entropy alloys. *Acta Mater.* **259**, 119240 (2023).

169. Lin, C. L. et al. Investigation on the thermal expansion behavior of FeCoNi and $Fe_{30}Co_{30}Ni_{30}Cr_{10-x}Mn_x$ high entropy alloys. *Mater. Chem. Phys.* **271**, 124907 (2021).

170. Tanimoto, H., Hozumi, R. & Kawamura, M. Electrical resistivity and short-range order in rapid-quenched CrMnFeCoNi high-entropy alloy. *J. Alloy. Compd.* **896**, 163059 (2022).

171. Pal, S., Nair, R. B. & McDonald, A. Toward understanding the microstructure and electrical resistivity of thermal-sprayed high-entropy alloy coatings. *J. Mater. Sci.* **57**, 20928–20944 (2022).

172. Kitagawa, J. Magnetic properties, electrical resistivity, and hardness of high-entropy alloys FeCoNiPd and FeCoNiPt. *J. Magn. Magn. Mater.* **563**, 170024 (2022).

173. Zhu, S. et al. A strong ferritic high-resistivity multicomponent alloy with tunable ordered coherent multicomponent nanoprecipitates. *Acta Mater.* **238**, 118209 (2022).

174. Kao, Y. F. et al. Electrical, magnetic, and Hall properties of $Al_xCoCrFeNi$ high-entropy alloys. *J. Alloy. Compd.* **509**, 1607–1614 (2011).

175. Chou, H. P., Chang, Y. S., Chen, S. K. & Yeh, J. W. Microstructure, thermophysical and electrical properties in $Al_xCoCrFeNi$ ($0 \le x \le 2$) high-entropy alloys. *Mater. Sci. Eng. B* **163**, 184–189 (2009).

176. Li, P., Wang, A. & Liu, C. T. Composition dependence of structure, physical and mechanical properties of $FeCoNi(MnAl)_x$ high entropy alloys. *Intermetallics* **87**, 21–26 (2017).

177. Chen, S.-K. & Kao, Y.-F. Near-constant resistivity in 4.2–360 K in a B2 $Al_{2.08}CoCrFeNi$. *AIP Adv.* **2**, 012111 (2012).

178. Bardeen, J., Cooper, L. N. & Schrieffer, J. R. Theory of superconductivity. *Phys. Rev.* **108**, 1175–1204 (1957).

179. Mizuguchi, Y., Kasem, M. R. & Matsuda, T. D. Superconductivity in $CuAl_2$-type $Co_{0.2}Ni_{0.1}Cu_{0.1}Rh_{0.3}Ir_{0.3}Zr_2$ with a high-entropy-alloy transition metal site. *Mater. Res. Lett.* **9**, 141–147 (2021).

180. Marik, S. et al. Superconductivity in a new hexagonal high-entropy alloy. *Phys. Rev. Mater.* **3**, 060602 (2019).

181. Liu, B. et al. Superconductivity and paramagnetism in Cr-containing tetragonal high-entropy alloys. *J. Alloy. Compd.* **869**, 159293 (2021).

182. Uporov, S. A. et al. Pressure effects on electronic structure and electrical conductivity of TiZrHfNb high-entropy alloy. *Intermetallics* **140**, 107394 (2022).

183. El-Atwani, O. et al. Outstanding radiation resistance of tungsten-based high-entropy alloys. *Sci. Adv.* **5**, eaav2002 (2024).

184. Orhan, O. K., Hendy, M. & Ponga, M. Electronic effects on the radiation damage in high-entropy alloys. *Acta Mater.* **244**, 118511 (2023).

185. Cusentino, M. A., Wood, M. A. & Dingreville, R. Compositional and structural origins of radiation damage mitigation in high-entropy alloys. *J. Appl. Phys.* **128**, 125904 (2020).

186. Levenets, A. V., Tikhonovsky, M. A., Voyevodin, V. N., Shepelev, A. G. & Nemashkalo, O. V. High-entropy alloys as a prospective class of new radiation-tolerant materials research development analysis based on the information databases. *Voprosy Atomnoj Nauki Tekhniki* https://doi.org/10.46813/2021-132-003 (2021).

187. Zhang, H. et al. Effects of nitrogen doping on microstructures and irradiation resistance of Ti–Zr–Nb–V–Mo refractory high-entropy alloy. *Acta Metall. Sin.* https://doi.org/10.1007/s40195-024-01686-0 (2024).

188. Kombaiah, B. et al. Nanoprecipitates to enhance radiation tolerance in high-entropy alloys. *ACS Appl. Mater. Interfaces* **15**, 3912–3924 (2023).

189. Deluigi, O. R. et al. Simulations of primary damage in a high entropy alloy: probing enhanced radiation resistance. *Acta Mater.* **213**, 116951 (2021).

190. Lin, Y. et al. Enhanced radiation tolerance of the Ni-Co-Cr-Fe high-entropy alloy as revealed from primary damage. *Acta Mater.* **196**, 133–143 (2020).

191. Tunes, M. A. et al. From high-entropy alloys to high-entropy ceramics: the radiation-resistant highly concentrated refractory carbide (CrNbTaTiW)C. *Acta Mater.* **250**, 118856 (2023).

192. Mañosa, L. & Planes, A. Elastocaloric effect in shape-memory alloys. *Shape Mem. Superelast.* https://doi.org/10.1007/s40830-024-00477-x (2024).

193. Zarnetta, R. et al. Identification of quaternary shape memory alloys with near-zero thermal hysteresis and unprecedented functional stability. *Adv. Funct. Mater.* **20**, 1917–1923 (2010).

194. Chen, H. et al. Unprecedented non-hysteretic superelasticity of [001]-oriented NiCoFeGa single crystals. *Nat. Mater.* **19**, 712–718 (2020).

195. Tanaka, Y. et al. Ferrous polycrystalline shape-memory alloy showing huge superelasticity. *Science* **327**, 1488–1490 (2010).

196. Omori, T. et al. Superelastic effect in polycrystalline ferrous alloys. *Science* **333**, 68–71 (2011).

197. Firstov, G. S., Kosorukova, T. A., Koval, Y. N. & Odnosum, V. V. High entropy shape memory alloys. *Mater. Today Proc.* **2**, S499–S503 (2015).

198. Firstov, G. S., Kosorukova, T. A., Koval, Y. N. & Verhovlyuk, P. A. Directions for high-temperature shape memory alloys' improvement: straight way to high-entropy materials? *Shape Mem. Superelast.* **1**, 400–407 (2015).

199. Piorunek, D. et al. Effect of off-stoichiometric compositions on microstructures and phase transformation behavior in Ni–Cu–Pd–Ti–Zr–Hf high entropy shape memory alloys. *J. Alloy. Compd.* **857**, 157467 (2021).

200. He, S. et al. Interpretable machine learning workflow for evaluation of the transformation temperatures of TiZrHfNiCoCu high entropy shape memory alloys. *Mater. Des.* **225**, 111513 (2023).

201. Thiercelin, L., Peltier, L. & Meraghni, F. Physics-informed machine learning prediction of the martensitic transformation temperature for the design of 'NiTi-like' high entropy shape memory alloys. *Comput. Mater. Sci.* **231**, 112578 (2024).

202. Akrami, S. et al. Defective high-entropy oxide photocatalyst with high activity for CO_2 conversion. *Appl. Catal. B* **303**, 1–24 (2022).

203. Xin, Y. et al. High-entropy alloys as a platform for catalysis: progress, challenges, and opportunities. *ACS Catal.* **10**, 11280–11306 (2020).

204. Löffler, T. et al. Discovery of a multinary noble metal–free oxygen reduction catalyst. *Adv. Energy Mater.* **8**, 1802269 (2018).

205. Yao, Y. et al. Carbothermal shock synthesis of high-entropy-alloy nanoparticles. *Science* **359**, 1489–1494 (2018).

206. Batchelor, T. A. A. et al. High-entropy alloys as a discovery platform for electrocatalysis. *Joule* **3**, 834–845 (2019).

207. Yao, Y. et al. High-entropy nanoparticles: synthesis–structure–property relationships and data-driven discovery. *Science* **376**, eabn3103 (2023).

208. Zhang, Y., Wang, D. & Wang, S. High-entropy alloys for electrocatalysis: design, characterization, and applications. *Small* **18**, 2104339 (2022).

209. Ren, J.-T., Chen, L., Wang, H.-Y. & Yuan, Z.-Y. High-entropy alloys in electrocatalysis: from fundamentals to applications. *Chem. Soc. Rev.* **52**, 8319–8373 (2023).

210. Schweidler, S. et al. High-entropy materials for energy and electronic applications. *Nat. Rev. Mater.* **9**, 266–281 (2024).

211. Sun, Y. & Dai, S. High-entropy materials for catalysis: a new frontier. *Sci. Adv.* **7**, eabg1600 (2024).

212. Wang, X., Guo, W. & Fu, Y. High-entropy alloys: emerging materials for advanced functional applications. *J. Mater. Chem. A Mater.* **9**, 663–701 (2021).

213. Mints, V. A., Svane, K. L., Rossmeisl, J. & Arenz, M. Exploring the high-entropy oxide composition space: insights through comparing experimental with theoretical models for the oxygen evolution reaction. *ACS Catal.* **14**, 6936–6944 (2024).

214. Batchelor, T. A. A. et al. Complex-solid-solution electrocatalyst discovery by computational prediction and high-throughput experimentation. *Angew. Chem. Int. Ed.* **60**, 6932–6937 (2021).

215. Clausen, C. M., Nielsen, M. L. S., Pedersen, J. K. & Rossmeisl, J. Ab initio to activity: machine learning-assisted optimization of high-entropy alloy catalytic activity. *High Entropy Alloy. Mater.* https://doi.org/10.1007/s44210-022-00006-4 (2022).

216. Yao, Y. et al. Extreme mixing in nanoscale transition metal alloys. *Matter* **4**, 2340–2353 (2021).

217. Li, T. et al. Denary oxide nanoparticles as highly stable catalysts for methane combustion. *Nat. Catal.* **4**, 62–70 (2021).

218. Priamushko, T., Kormányos, A. & Cherevko, S. What do we know about the electrochemical stability of high-entropy alloys? *Curr. Opin. Chem. Eng.* **44**, 101020 (2024).

219. Kormányos, A. et al. Stability of high-entropy alloys under electrocatalytic conditions. *iScience* **26**, 107775 (2023).

220. De Vrieze, J. E., Gunasooriya, G. K. K., Thybaut, J. W. & Saeys, M. Operando computational catalysis: shape, structure, and coverage under reaction conditions. *Curr. Opin. Chem. Eng.* **23**, 85–91 (2019).

221. Gao, S. et al. Synthesis of high-entropy alloy nanoparticles on supports by the fast moving bed pyrolysis. *Nat. Commun.* **11**, 2016 (2020).

222. Tao, L. et al. A general synthetic method for high-entropy alloy subnanometer ribbons. *J. Am. Chem. Soc.* **144**, 10582–10590 (2022).

223. Wei, J. et al. Deep eutectic solvent assisted facile synthesis of low-dimensional hierarchical porous high-entropy oxides. *Nano Res.* **15**, 2756–2763 (2022).

224. Dangwal, S. & Edalati, K. High-entropy alloy $TiV_2ZrCrMnFeNi$ for hydrogen storage at room temperature with full reversibility and good activation. *Scr. Mater.* **238**, 115774 (2024).

225. Ma, X. et al. Study on microstructure and the hydrogen storage behavior of a TiVZrNbFe high-entropy alloy. *Intermetallics* **157**, 107885 (2023).

226. Shahi, R. R., Gupta, A. K. & Kumari, P. Perspectives of high entropy alloys as hydrogen storage materials. *Int. J. Hydrog. Energy* **48**, 21412–21428 (2023).

227. Mohammadi, A. et al. High-entropy hydrides for fast and reversible hydrogen storage at room temperature: binding-energy engineering via first-principles calculations and experiments. *Acta Mater.* **236**, 118117 (2022).

228. Moore, C. M. et al. Hydrogen accommodation in the TiZrNbHfTa high entropy alloy. *Acta Mater.* **229**, 117832 (2022).

229. Sahlberg, M., Karlsson, D., Zlotea, C. & Jansson, U. Superior hydrogen storage in high entropy alloys. *Sci. Rep.* **6**, 36770 (2016).

230. Chen, S. K., Lee, P. H., Lee, H. & Su, H. T. Hydrogen storage of C14-$Cr_uFe_vMn_wTi_xV_yZr_z$ alloys. *Mater. Chem. Phys.* **210**, 336–347 (2018).

231. Edalati, P. et al. Reversible room temperature hydrogen storage in high-entropy alloy TiZrCrMnFeNi. *Scr. Mater.* **178**, 387–390 (2020).

232. Andrade, G. et al. Crystal structure and hydrogen storage properties of AB-type TiZrNbCrFeNi high-entropy alloy. *Int. J. Hydrog. Energy* **48**, 13555–13565 (2023).

233. Edalati, K. et al. Design and synthesis of a magnesium alloy for room temperature hydrogen storage. *Acta Mater.* **149**, 88–96 (2018).

234. Shang, Y. et al. Ultra-lightweight compositionally complex alloys with large ambient-temperature hydrogen storage capacity. *Mater. Today* **67**, 113–126 (2023).

235. Marques, F., Balcerzak, M., Winkelmann, F., Zepon, G. & Felderhoff, M. Review and outlook on high-entropy alloys for hydrogen storage. *Energy Env. Sci.* **14**, 5191–5227 (2021).

236. Felderhoff, M., Weidenthaler, C., von Helmolt, R. & Eberle, U. Hydrogen storage: the remaining scientific and technological challenges. *Phys. Chem. Chem. Phys.* **9**, 2643–2653 (2007).

237. Weidenthaler, C. & Felderhoff, M. Solid-state hydrogen storage for mobile applications: quo vadis? *Energy Env. Sci.* **4**, 2495–2502 (2011).

238. Kumbhakar, M. et al. High-throughput screening of high-entropy fluorite-type oxides as potential candidates for photovoltaic applications. *Adv. Energy Mater.* https://doi.org/10.1002/aenm.202204337 (2023).

239. Suhr, E. et al. High-throughput exploration of structural and electrochemical properties of the high-entropy nitride system (Ti–Co–Mo–Ta–W)N. *Adv. Eng. Mater.* **25**, 2300550 (2023).

240. He, C. Y. et al. Scalable and highly efficient high temperature solar absorber coatings based on high entropy alloy nitride AlCrTaTiZrN with different antireflection layers. *J. Mater. Chem. A* **9**, 6413–6422 (2021).

241. Khan, M., Rahaman, M. Z. & Ali, M. L. Pressure-induced band gap engineering of nontoxic lead-free halide perovskite $CsMgI_3$ for optoelectronic applications. *ACS Omega* **8**, 24942–24951 (2023).

242. Wang, S.-P. & Xu, J. TiZrNbTaMo high-entropy alloy designed for orthopedic implants: as-cast microstructure and mechanical properties. *Mater. Sci. Eng. C* **73**, 80–89 (2017).

243. Castro, D., Jaeger, P., Baptista, A. C. & Oliveira, J. P. An overview of high-entropy alloys as biomaterials. *Metals* **11**, 648 (2021).

244. de Oliveira, T. G., Fagundes, D. V., Capellato, P., Sachs, D. & da Silva, A. A. A. P. A review of biomaterials based on high-entropy alloys. *Metals* **12**, 1940 (2022).

245. Shi, Z., Fang, Q., Liaw, P. K. & Li, J. Corrosion-resistant biomedical high-entropy alloys: a review. *Adv. Eng. Mater.* **25**, 2300968 (2023).

246. Rashidy Ahmady, A. et al. High entropy alloy coatings for biomedical applications: a review. *Smart Mater. Manuf.* **1**, 100009 (2023).

247. Feng, J. et al. Preparation of TiNbTaZrMo high-entropy alloy with tunable Young's modulus by selective laser melting. *J. Manuf. Process.* **85**, 160–165 (2023).

248. Yang, W. et al. Design and properties of novel Ti–Zr–Hf–Nb–Ta high-entropy alloys for biomedical applications. *Intermetallics* **141**, 107421 (2022).

249. Popescu, G. et al. New TiZrNbTaFe high entropy alloy used for medical applications. *IOP Conf. Ser. Mater. Sci. Eng.* **400**, 022049 (2018).

250. Shittu, J. et al. Biocompatible high entropy alloys with excellent degradation resistance in a simulated physiological environment. *ACS Appl. Bio Mater.* **3**, 8890–8900 (2020).

251. Motallebzadeh, A. et al. Microstructural, mechanical and electrochemical characterization of TiZrTaHfNb and $Ti_{1.5}ZrTa_{0.5}Hf_{0.5}Nb_{0.5}$ refractory high-entropy alloys for biomedical applications. *Intermetallics* **113**, 106572 (2019).

252. Hori, T., Nagase, T., Todai, M., Matsugaki, A. & Nakano, T. Development of non-equiatomic Ti–Nb–Ta–Zr–Mo high-entropy alloys for metallic biomaterials. *Scr. Mater.* **172**, 83–87 (2019).

253. Takahashi, M., Sato, K., Togawa, G. & Takada, Y. Mechanical properties of Ti–Nb–Cu alloys for dental machining applications. *J. Funct. Biomater.* **13**, 263 (2022).

254. Zhou, E. et al. A novel Cu-bearing high-entropy alloy with significant antibacterial behavior against corrosive marine biofilms. *J. Mater. Sci. Technol.* **46**, 201–210 (2020).

255. Raabe, D., Tasan, C. C. & Olivetti, E. A. Strategies for improving the sustainability of structural metals. *Nature* **575**, 64–74 (2019).

256. Raabe, D. The materials science behind sustainable metals and alloys. *Chem. Rev.* **123**, 2436–2608 (2023).

257. Zhang, Z., Tang, H. & Xu, Z. Fatigue database of complex metallic alloys. *Sci. Data* **10**, 447 (2023).

Review article

258. Wang, W. et al. Automated pipeline for superalloy data by text mining. *NPJ Comput. Mater.* **8**, 9 (2022).
259. Zhou, Z. et al. Machine learning guided appraisal and exploration of phase design for high entropy alloys. *NPJ Comput. Mater.* **5**, 128 (2019).
260. Gutfleisch, O. et al. Magnetic materials and devices for the 21st century: stronger, lighter, and more energy efficient. *Adv. Mater.* **23**, 821–842 (2011).
261. Torrubia, J., Valero, A. & Valero, A. Energy and carbon footprint of metals through physical allocation. Implications for energy transition. *Resour. Conserv. Recycl.* **199**, 107281 (2023).

Author contributions
L.H., Z.L., A.L., O.G. and D.R. developed the ideas for the paper. All authors contributed equally to the concept, discussion of the results and manuscript writing.

Competing interests
The authors declare no competing interests.

Additional information
Supplementary information The online version contains supplementary material available at https://doi.org/10.1038/s41578-024-00720-y.

Peer review information *Nature Reviews Materials* thanks Qihong Fang and the other, anonymous, reviewer(s) for their contribution to the peer review of this work.

Publisher's note Springer Nature remains neutral with regard to jurisdictional claims in published maps and institutional affiliations.